ABSTRACT

Title of Dissertation: NANOPATTERNED BLOCK COPOLYMERS FOR USE AS VASCULAR BIOMATERIALS

Joshua S. Silverstein, Doctor of Philosophy, 2012

Directed By: Professor Peter Kofinas
Fischell Department of Bioengineering

Manipulation of surface topography or chemistry has been a growing trend in efforts to enhance the properties of medical devices. Understanding the interactions of biomolecules with nanoengineered surfaces is vital to assess the safety and efficacy of devices that incorporate these structures. In this dissertation, a model block copolymer (BCP) system based on poly(styrene)-block-poly(1,2-butadiene) was systematically modified using photochemical thiol-ene chemistry. Poly(1,2-butadiene) molecular weight and thiol-ene ratios were systematically varied based on a model monomer, boc-cysteamine, to determine the efficiency of the reaction.

The results demonstrate the polydispersity index of modified BCPs significantly increased when low thiol-ene ratios were employed and sometimes induced gelation of the reacted polymers. Using a tenfold excess of thiol, functionalizations between 60-90% were obtained for an acid, amine, amide, and a pharmaceutical with a

pendant thiol. Calorimetry showed a 30-60 °C increase in the glass transition temperature of the daughter polymers. Subsequently, films were cast from solvents found suitable to forming self-assembled BCP thin films. The synthetic and processing approach allows for the formation of nanopatterned block copolymer films with controlled chemistries from a single source material.

The BCPs were further characterized using water contact angle measurements and atomic force microscopy in liquid. Significantly decreased contact angles were caused by selective swelling of charged BCP domains. Protein (fibrinogen, albumin, cytochrome C, immunoglobulin G) adsorption experiments were conducted under static and dynamic conditions with a quartz crystal microbalance with dissipation. The results indicate that nanopatterned chemistry and experimental conditions strongly impact adsorption dynamics. Adsorption behavior was dependent both on protein structure and the characteristics of the surface. Depending on the structural stability of the protein, polyelectrolyte surfaces significantly increased adsorption over uncharged controls.

NANOPATTERNED BLOCK COPOLYMERS FOR USE AS VASCULAR BIOMATERIALS

By

Joshua S. Silverstein

Dissertation submitted to the Faculty of the Graduate School of the
University of Maryland, College Park, in partial fulfillment
of the requirements for the degree of
Doctor of Philosophy
2012

Advisory Committee:
Professor Peter Kofinas, Chair
Professor Helim Aranda-Espinoza
Professor Robert M. Briber
Dr. Benita J. Dair
Professor John P. Fisher

Dedication

In memory of my grandparents,

Julius and Esther Waskow

Arnold and Selma Silverstein

Acknowledgements

I first thank my family, Mom, Dad, Jeremy, and Joel for their love and support over the years. I could not have made it without you guys.

I'm grateful to my future wife and best friend, Paulina, whose wisdom, beauty, humor, and patience helped get me through the tough days. I am also indebted to Gregory and Yelena Nusinovich, who accepted me as a prospective son-in-law with kindness and Russian hospitality.

Thank you to Prof. Peter Kofinas, who advised me for many years and is more patient than I probably deserved. I'll never forget all you've done for me and will always remember Festivus dinners, coffee breaks, and lunchtime shenanigans. I was fortunate to have Dr. Beni Dair as my FDA advisor and I am very appreciative for her support, knowledge, and the friendly reminder that a scientist's education is never complete, even after the Ph.D. defense. I'm grateful to Dr. Briber for serving on my committee and providing insight into my project at key moments. Thanks go to Prof. Helim Aranda-Espinoza and Prof. John Fisher for agreeing to be on my committee, use of their resources, and applying the right pressure.

I'd like to thank my past and present colleagues and friends from the Kofinas Lab, including Aaron, Adam, Angela, Angela, Brendan, Irene, Omar, Mert, Pinar, Von, Dan, Linden, and Ta-I "G-Money". I'd like to thank the undergraduates who helped me along the way and in the great tradition; most of your work remains unsung. I'm grateful to members of Dr. Briber's lab, with whom we shared group meetings and discussions. Special thanks go to Xin Zhang, who was always helpful with physics, instrumentation, philosophy, and his knowledge of rock n roll.

I am thankful to OSEL senior staff for their unyielding support. Specifically, Charles Warr and Steve Pollack for the privilege of completing my dissertation work at FDA. Additional gratitude goes to Dinesh Patwardhan for his support, insight, and encouragement. I'd like to thank my DCMS colleagues and supervisors, who are too numerous to name, including the minions of students who humored me throughout the years. Thanks to my friend, golf partner, and collaborator Brendan Casey for pushing me at the end. Additionally, I extend gratitude to Eric Sussman for the review of my dissertation. Finally, special thanks to the Nanotoxicology and Active Materials Laboratories for their insight, criticism, and riveting lunchtime conversations.

This project was supported by an appointment to the University Participation Program at the Center for Devices and Radiological Health administered by the Oak Ridge Institute for Science and Education through an interagency agreement between the U.S. Department of Energy and the U.S. Food and Drug Administration.

So long, and thanks for all the fish.

Table of Contents

List of Figures

List of Tables

1 Introduction

1.1 Significance

Nanoengineered materials are increasingly investigated for use in biomedical devices, imaging, in-vitro diagnostics, and drug-delivery systems by the properties attributable to their dimensions.[1] Engineered nanomaterials include nanoparticles, aggregates, nanotextured surfaces, and nanofibers. Chemical or topographical modification on the surface contacting the physiological environment is seen as a method to enhance the biocompatibility of blood contacting devices such as stents, grafts, oxygenators, pacemaker leads, and catheters.[2] Some methods to fabricate or process nanotextured surfaces are chemical etching of metals, lithographic processes, or use of self-assembled systems such as block copolymers (BCPs).

The difficulty of nanomaterial testing was highlighted in recent reviews and remains a concern for academics, industry, and regulators.[3] While clinical data remains the biocompatibility gold standard as highlighted in ISO-10993, *in vitro* data is gaining traction due to cost economy and high throughput analytical methods. However, disagreements within the community concerning preliminary aspects of biocompatibility such as protein adsorption still persist. The comparison of results from dissimilar materials and proteins could explain ambiguous results from distinct studies. Therefore, the definition of a model system where chemistry can be systematically altered may contribute to this knowledge base and help in the development of standardized testing methods for nanomaterial analysis.

In fact, BCP materials penetrated the interventional cardiovascular device market in 2002 with the approval of Taxus, which has a BCP coating used for the controlled release of a therapeutic. An analog to the poly(styrene)-block-poly(isobutylene)-block-poly(styrene) (SIBS) biomedical polymer was used in this dissertation to develop a model system where the chemistry could be systematically varied within a BCP pattern. While chemical reactions on the styrene block of SIBS are possible, wide scoped synthetic schemes are not feasible and the reagents often present health or environmental concerns.

This dissertation describes a modular synthetic approach using thiol-ene photochemistry, which resulted in the successful modification of poly(styrene)-block-poly(1,2-butadiene) (PS/PB) with various functional groups, including an acid, amide, amine, and an anti-hypertensive pharmaceutical. This system was characterized with surface and bulk techniques to assess the reaction yields and resultant polymer properties after thiol addition. Subsequently, this model system was used to determine how BCP morphologies affected the adsorption of proteins with varying charge and structure.

1.2 Project Goals

The objectives of this research were:

1. The synthesis and characterization of a nanopatterned BCP library with systematically modified functional groups and description of how the synthesis process altered the properties of these polymers.
2. The understanding of how chemically distinct BCP morphologies affect the adsorption of proteins with altered charge, size, and stability.

The methods used to achieve these objectives:

1. Systematic modification of PS/PB BCPs was completed using photochemical thiol-ene reactions to graft an acid, amide, amine, and an anti-hypertensive pharmaceutical to the side chains of PB. ^{1}H nuclear magnetic resonance spectroscopy (NMR) and gel permeation chromatography (GPC) were utilized to obtain quantitative measurements of the degree of functionalization and the polydispersity index (PDI). Differential scanning calorimetry was employed to describe the resulting thermal properties of thiol grafted BCPs. The surface morphologies of the PS/PB BCPs were imaged using atomic force microscopy (AFM).
2. Contact angle goniometry measurements were used to determine the role of grafted thiols on the surfaces' wettability. Further AFM imaging was used to compliment contact angle measurements and evaluate the swelling of the surfaces after exposure to phosphate buffer. Finally, a quartz crystal microbalance with dissipation monitoring (QCM-D) was used to quantify protein adsorption and qualify the nature of the protein layer. Proteins with

varying charge, molecular weight (MW), and stability against denaturation were examined to understand whether nanopatterned BCPs surfaces affect protein adsorption. Experiments were completed under both static and dynamic conditions to determine whether the testing method affected the nature of the protein adlayer.

The results of these experiments indicated that:

1. Preliminary experiments showed that low thiol-ene ratios on high MW BCPs increased the PDI and sometimes induced gelation, as confirmed by GPC. NMR spectra revealed that large amounts of excess thiol were required to obtain high functionalization degrees on high MW PS/PB BCPs. Using large excess thiol concentrations, high functionalization degrees were obtained and resulted in the modification of PS/PB with an acid, amide, amine, and a pharmaceutical compound. DSC indicated that large changes in the glass transition temperature (T_g) resulted from the modification process due to lost configurational entropy and free volume in the products. BCP nanostructures were successfully processed from spin coating and imaged using AFM using solvents found suitable through an iterative technique.
2. Static contact angle measurements confirmed that the grafting process induced large wetting differences. Liquid AFM measurements corroborated that wetting differences occurred due to selective swelling of the BCPs grafted with charged monomers. The results from QCM-D experiments indicated that

significant differences were observed between static and dynamic adsorptions. The use of proteins with different charges, MW, and stability against denaturation confirmed that the interactions between proteins and BCP nanopatterns are dependent on protein properties and the surfaces.

1.3 Background

1.3.1 Blood Contacting Medical Devices

Medical devices often contact blood and other physiologic fluids throughout their normal use. Short-term blood contacting devices include catheters, angioplasty balloons, and blood transfusion bags. Devices implanted for long periods in patients include vascular stents, grafts, oxygenators, pacemakers, and defibrillators. Despite hermetically sealed metal encasements for pacemakers and defibrillators, electric leads connect to the heart and involve incidental contact with blood.[4] The fouling of blood contacting medical devices by proteins, small molecules, and various cellular phenotypes may result in diminished effectiveness or result in adverse events such as myocardial infarction.[5]

The use of foreign materials may adversely affect patient health from contact during surgery or during a device's regular lifetime in the case of long-term implants. In fact, the wide scope of blood contacting medical devices and varying conditions in which they are utilized suggests that a systematic study of biofouling is required. Since the aforementioned medical devices contact blood both under static and dynamic

conditions, evaluating these situations could aid in the development of risk assessments and *in vitro* methods for standard development.

Material biocompatibility determination remains challenging despite numerous revisions to ISO-10993, owing to the wide scope of medical devices.[6] The suggested tests for implanted blood contacting devices such as vascular stents and grafts include thrombosis and hematology studies using either *in vitro* or clinical *in vivo* methods. These may include, but are not limited to, thrombus gravimetry, percent occlusion from clinical studies, and optical/electron microscopy to examine the implant for leukocyte and platelet adhesion.

Regardless of contact duration, an inflammatory response initiates when a device perturbs the physiological environment and causes injury. The host reaction to foreign materials proceeds as following: injury, acute inflammation, chronic inflammation, granulation tissue, foreign body reaction, and fibrosis.[7] In the specific case of blood contacting materials, the interplay between plasma proteins, platelets, and surface characteristics will help determine the physiological response. Platelets are anuclear cells approximately 4 μm in diameter and disc shaped at rest. Upon activation, platelets change shape and extend pseudopodia that augment their ability to form a hemostatic clot, as shown in the scanning electron microgram Figure 1.1. Platelets require Ca^{2+}, fibrinogen, and a conformational change in the GP IIb/IIIa receptor to form the aggregate making up a thrombus. Platelet adhesion or activation in response to a medical device can cause coagulation and may lead to an occlusion (blockage), ending in device failure and potential patient mortality.[8]

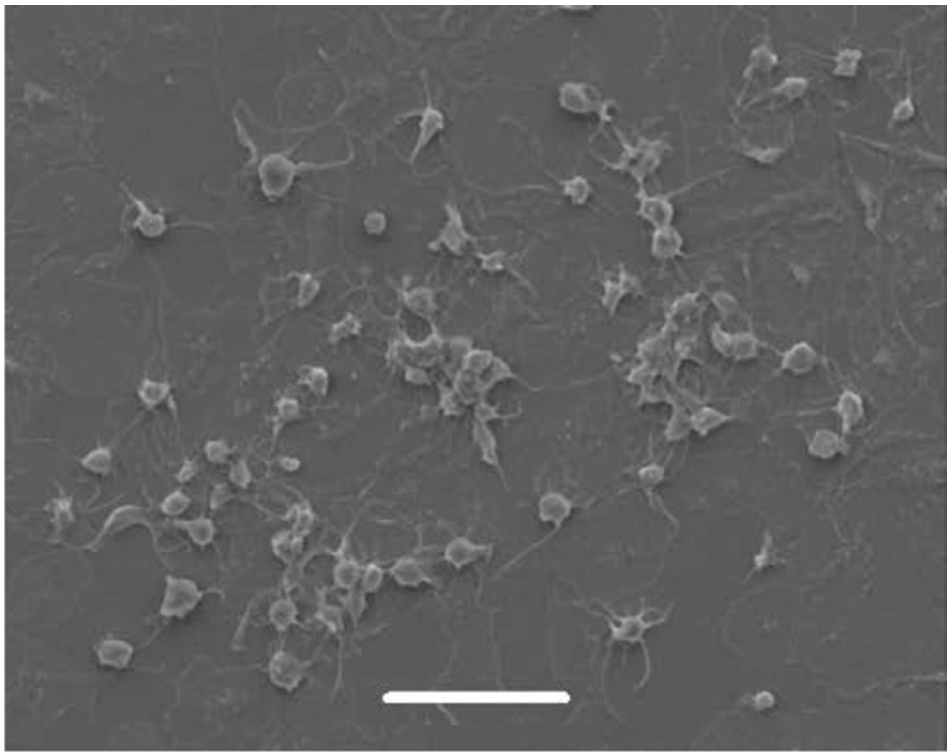

Figure 1.1. Scanning electron micrograph of human platelets on a block copolymer surface. Scale bar: 10 µm. (Silverstein J.S., unpublished data).

Fibrinogen's role in the coagulation cascade underlines the importance of understanding protein adsorption. After injury, protein adsorption is one of the primary events establishing the physiological response to implanted materials and is a major factor in determining either successful tissue integration or adverse reaction.[9] The fouling of foreign materials by proteins or small molecules may result in reduced or diminished effectiveness.[10] For the case of electrical leads, lower signal strength may occur after biofouling .[11] Additionally, adsorbed plasma proteins involved in the coagulation cascade such as fibrinogen or von Willebrand's factor can increase platelet adhesion on synthetic polymeric surfaces.[12] Platelet adhesion on implants may result in a thrombotic event, which may cause heart attacks, or myocardial

infarction.[13] Cleavage of the fibrinogen chain by thrombin has been established as a major factor in the onset of coagulation.[14] Considering that structural changes may occur when proteins adsorb to a surface, their study may serve as an indirect method for determining a material's propensity to induce coagulation.

1.3.2 Protein Adsorption

Despite decades of research, there is disparity describing substrate effects on protein adsorption.[9] Numerous methods have been developed or utilized to define protein adsorption on the surface of synthetic or natural substrates. Before assessing the merit of each approach, the structure and properties of proteins will be introduced with a consideration of the physical interactions arising as a protein contacts a synthetic surface.

Proteins are biomacromolecules consisting of a subset of 20 different amino acid (AAs) linked by peptide bonds. The sequence of AAs within a protein is described as the primary structure, which is equivalent to the chain architecture described in Chapter 1.4.1.[15] The AAs making up proteins have distinctive solution properties on their side chains, including polarity, charge, and hydrophobicity. The combination of weak non-covalent interactions and the hydrophobic effect induces the self-assembly of motifs into structures such as α–helices and β–sheets, which are defined as secondary structures. The grouping of secondary structures from one polypeptide chain forms the tertiary structure. If a protein consists of more than one polypeptide chain, the assembly of tertiary structures is described as the quaternary structure.[15]

Proteins are often classified by their shape and aqueous solubility.[15] Globular proteins, such as albumin, hemoglobin, and immunoglobulins are water soluble and found in circulation. Fibrous proteins such as actin, collagen, and keratin typically are insoluble in water and form connective tissues in the body. This discussion will be limited to globular proteins since they are primarily found in blood, unlike fibrous proteins.

Proteins are also categorized by their isoelectric point (pI), which is the pH where the overall charge is neutral.[15] When solution pH is above the pI, proteins have overall negative charge. Likewise, proteins with a pI larger than the solution pH are positively charged. For example, human fibrinogen has a pI of 5.5, thus at physiological pH 7.4 it is a negatively charged protein.[16] Understanding the pI is vital to the determination of proteins interactions with surfaces, which often consist of heterogeneous polarities or charges themselves. However, charge anisotropy is present on proteins and the pI should only be considered an additive measure of charge patches.[17]

When a protein solution contacts a surface, several events must be considered. Primarily, diffusion or convection of proteins occurs from the bulk solution towards the solid-liquid interface.[18] Under diffusion controlled adsorption, the bulk concentration gradient in the solution drives protein diffusion towards the interface. Diffusion mediated adsorption is related to the square root of time.

Following diffusion, protein adsorption occurs, which is historically described by the Langmuir isotherm model:[18]

$$v_s = \frac{kA}{1 + kA}$$

Where v_s=mole/area of adsorbent, k=rate constant, and A=bulk solute concentration

The Langmuir model has a number of preconditions, including a monolayer assumption, surface homogeneity, no competitive adsorption, dilute solution, and reversibility. While this model was useful for characterizing protein adlayer formation, adsorption processes are rarely reversible on the surface of hydrophobic polymers, such as those encompassing medical devices.[18]

After the initial adsorption process structural changes within the protein adlayer may occur including partial denaturation. This is especially prevalent when investigating hydrophobic proteins such as serum albumin on hydrophobic polymers.[18] Several mechanisms have been proposed that describe the physical processes driving adsorption induced conformational changes for hydrophobic polymer and protein systems. Dehydration may occur from bonding of complimentary hydrophobic domains on each respective structures.[19] Dehydration increases protein's entropy through the structural changes occurring during denaturation. These structural changes represent some degree of denaturation, which can induce coagulation in the case of fibrinogen.[20]

Electrostatics certainly plays a role in the adsorption process, yet their contribution is still not well established. Results often conflict with electrostatic arguments of repulsion between a negatively charged protein and polymer. Several mechanisms for like-charged attraction between proteins and surfaces have been proposed. The

availability of anionic and cationic species in buffers may provide a counter ion bridge between like-charged proteins and surfaces.[18] Additionally, the pI of a protein is a parameter that is the additive contribution of charged amino acids. Thus, there are distinct regions within a negatively charged protein consisting of cationic segments.[19] Electrostatics can play a decisive role in the adsorption of rigid proteins since their hydrophobic domains are less likely to become exposed upon adsorption.[19]

Considering the numerous parameters participating in protein adsorption, thorough studies include the use of proteins with dissimilar pI, MW, and stability against denaturation. Among the most relevant to the study of blood contacting polymers are proteins present in plasma, which is the acellular component of blood. Typically, these would include fibrinogen, serum albumin, and immunoglobulin G (IgG).

1.3.2.1 Experimental Methods in Protein Adsorption

Labeling, spectroscopy, enzyme linked immunosorbent assays (ELISAs), surface plasmon resonance sensors (SPR), and the quartz crystal microbalance (QCM) have been used to characterize protein adsorption to varying degrees of success.[8, 21-25] These methods confer varying amounts of both qualitative and quantitative analysis. In this discussion, an attempt will be made to impartially describe the strengths and shortcomings of each approach to protein measurement.

Protein labeling using fluorophores such as fluorescein isothiocynate (FITC) is a facile method for investigating protein adlayers on material surfaces in a high throughput manner using a fluorescent plate reader. FITC tagged proteins are readily available from commercial chemical supply houses such as Sigma Aldrich or

Invitrogen. Additionally, kits for tagging proteins in-house with more stable fluorophores such as AlexaFluor are readily available from similar suppliers. However, fluorescent tags are frequently bulky conjugated Π-systems, which have significant hydrophobic properties. The hydrophobicity could potentially increase adsorption on hydrophobic polymers. Regardless, a protein's properties may become significantly altered by fluorescent tags. While some studies have validated unaltered adsorption properties of fluorescently tagged proteins, separate studies concluded that fluorophores indeed change the solution properties of proteins.[26, 27]

The use of radioactive isotopes such as ^{125}I is another label-based technique used to measure adsorbed protein layers. Before the advent of quality and cost effective fluorophores, radioactive isotopes were common in biology laboratories. While low isotope concentrations are typical, the main concern is the safety of laboratory workers. Often, contamination issues are present in laboratories using radioactive isotope based methods and health concerns continue. Increasingly, scintillation counters are being phased out and replaced with non-radioactive protocols.

ELISAs have been used to examine protein adlayers through established antibody-antigen binding events.[25] ELISAs for protein adsorption compare surfaces with unknown concentrations to a calibration curve from standardized serial dilutions of the antigen solution. In an iteration of ELISA, antibodies tagged with an enzyme such as horseradish peroxidase are developed with reagents such as hydrogen peroxide to provide colorimetric contrast read with a plate reader. ELISAs can be conducted in 96-well plates that permit the high throughput analysis necessary for rapid material screening. ELISAs assume that the antibody binding site of the antigen is available,

which may be inaccurate due to conformation changes arising from protein adsorption on synthetic surfaces.[28]

Spectroscopy techniques such as attenuated total reflectance Fourier transform infrared spectroscopy (ATR-FTIR), X-ray photoelectron spectroscopy (XPS), and circular dichroic spectroscopy have been used to examine protein adlayers.[29-31] The merits of spectroscopy techniques are that they confer conformational information about adsorbed protein layers, including the relative percentages of secondary motifs such as α-helices and β-sheets.[29] A disadvantage of the various spectroscopy techniques versus the aforementioned labeling techniques is their low sample throughput and sometimes require ultra-high vacuum (UHV). The UHV requirement for many spectroscopic techniques forbids examination of adlayers in aqueous media, which may introduce artifacts after sample preparation. Additionally, many spectroscopy techniques are incapable of providing quantitative information about adsorbed layers.

A surface plasmon resonance sensor (SPR) is a label-free technique to compare relative protein adsorption on surfaces. SPR works through the optical excitation of plasma waves on the surface of pristine noble metals such as gold or silver.[32] Transduction occurs through the altered refractive properties of the adsorbed layer. While SPR can detect infinitesimal chemisorption processes qualitatively, the pristine optical properties of the noble metal layer make their reusability difficult, especially in the case of polymer films. Additionally, an assumption of constant refractive indices is included with SPR experiments, which may not always be valid.[21]

1.3.2.2 Quartz Crystal Microbalance

QCM is an attractive option due to its ability to quantify adsorbed layers and provide some conformational information, while providing reusability of substrates absent in the SPR technique. QCM works by the application of an external driving circuit to a quartz crystal. Alternating current application to a quartz crystal causes vibrations due to the piezoelectric effect. Commercially available quartz crystals typically oscillate at a fundamental resonant frequency of 5 MHz. Quartz oscillators are advantageous due to their high Q-factor, which is approximated as the ratio of energy stored and dissipated during one oscillation. A formal definition of the inverse Q-factor, or dissipation, is discussed later in this section. The high Q-factor of quartz ensures that vibrational frequency is not damped and thus is less subject to drift than other piezoelectric materials.

Typical quartz crystal oscillators are AT-cut, which describes the orientation of the quartz crystal plane and are used to optimize manufacturing yield and performance. The AT-cut ensures that the mechanical shear induced during electric field application occurs in a central location on the crystal surface.[33] The resonance frequency at which quartz vibrates is defined as:[34]

$$f = n\frac{v_q}{2t_q} = nf_0$$

Where v_q=speed of sound, t_q=thickness of quartz (typically 300 µm), n=overtone, and f_0=fundamental frequency

Multiple resonance frequencies occur in quartz oscillators, which originate from the normal modes of vibration, also known as overtones. After replacement of the thickness, t_q, with m/ρ (mass/density), differentiation with respect to mass, and rearrangement results in a linear relationship between frequency and mass change when the mass of quartz is much greater than the adsorbed layer. This relationship was first described by Sauerbrey:[35]

$$\Delta m = -C\frac{\Delta f}{n}$$

Where C=constant (17.7 $ng \cdot cm^{-2} \cdot Hz^{-1}$), n=overtone, and Δf=change in frequency (Hz)

Conventional QCM with the Sauerbrey equation can be used for gravimetry with limitations less than 0.01 Hz in vacuum for the fundamental frequency, which corresponds to less than 1 ng/cm^2.[34] In liquid, the sensitivity is approximately 0.2 Hz, or ~20 ng/cm^2 according to the Sauerbrey equation. The high sensitivity of QCM in vacuum was used to quantify industrially used processes such as atomic layer deposition.[36] Outside of vacuum, QCM can be used to determine the thickness of films, assuming the coating is uniform and the crystal's frequency is measured both before and after processing.[37]

QCM measurements with the Sauerbrey equation provide thickness or mass quantities of solid films assuming uniform density. The sole use of frequency changes in conventional QCM limited the measurement of biological samples, which often

contain large amounts of bound hydration layers.[34] The reasons for reduced QCM performance in liquids are described in the succeeding paragraphs. Rodahl, Hook, and coworkers developed a novel QCM system in the 1990s introducing a dissipative measurement combined with the frequency changes typical of the QCM. This instrument was termed QCM with dissipative monitoring (QCM-D). The instrument used for this dissertation is shown in Figure 1.2 and consists of 4 distinct sample loops that can independently operate.

Figure 1.2. Picture of the quartz crystal microbalance with dissipation. Combined with a multichannel peristaltic pump, 4 samples can be run simultaneously (Courtesy of Q-Sense).

Dissipation is the inverse of the aforementioned Q-factor and is defined as:[38]

$$D = \frac{E_{dissipated}}{2\pi E_{stored}}$$

This term is not merely the ratio of energy lost through gravimetric increases, but the sum of all contributions to acoustic dissipation. When switching from vacuum/air to aqueous media, the higher viscosity causes significant damping of the oscillations. While a formal definition of the frequency and dissipation change from air to water will not be described, briefly, they are both functions of the fluid viscosity, density, quartz density and thickness.

Pertinent to this discussion of QCM-D is the data acquisition system used in this dissertation. The QCM-D used in this dissertation can rapidly open and close the driving circuit to measure frequency and dissipation. When the circuit is opened, frequency driving ceases, signal decay is measured, and fit to an exponentially damped sinusoid:[39]

$$A(t) = A_0 e^{t/\tau} \sin(\omega t + \varphi) + C, \text{ for } t \geq 0$$

Where A_0=Initial amplitude, t=time, τ=decay time constant, ω=angular frequency, φ=phase shift

The QCM-D can determine ω and τ through an algorithm incorporated within its software package, Q-Soft. With these parameters, the total signal dissipation can be calculated as:[39]

$$D_{total} = \frac{2}{\omega\tau}$$

Now that the signal processing techniques for the QCM-D were described, the technique for converting the raw dissipation value into an interpretation of mass will be discussed.

When considering an adlayer within a liquid medium on a crystal, there are several parameters that relate to structure. For the explicit case of an adsorbed protein, both the protein and its coupled hydration layer contribute to its structure. QCM without dissipative monitoring, as discussed previously, cannot recognize the hydration layer and translates the complex into a thickness. This would make QCM equivalent to an SPR technique despite dissimilar mechanisms of action (ie. vibrational vs. optical). Decoupling the dampening of quartz from the adlayer was a necessity for the development of QCM-D.

The model describing viscoelastic adlayers on quartz surfaces was described by Voinova et al.[40] The theory uses a Voigt viscoelastic model with a spring and dashpot operating in parallel. The Voigt model is shown schematically in Figure 1.3 with a generalized force/displacement versus time graph. The dissipation of the adlayer is described as a function of overtone, thickness, density, viscosity, and elasticity.

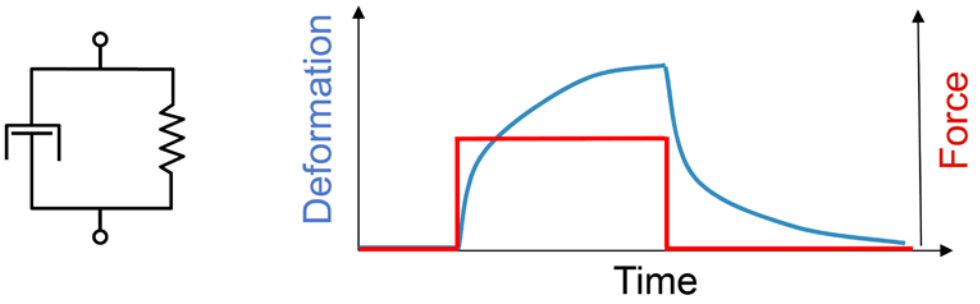

Figure 1.3. Spring and dashpot diagram of the Voigt model used to fit QCM-D data in this dissertation. The dashpot element causes non-linear deformation behavior upon force application and release

This discussion will now shift to experimental results and QCM-D approaches from various research groups. QCM-D has been shown to more accurately estimate mass in liquids than the Sauerbrey relation due to consideration of adlayer viscoelastic properties.[41] The constant switching of the drive circuit permits real-time measurement of adlayers and affords both frequency and dissipation data within short time scales (approximately 3 Hz).

QCM-D has been used to describe the solution and mechanical properties of polyelectrolyte multilayers (PEM), polymer brushes, lipids, and nanoparticles.[42, 43] Specifically, QCM-D was able to determine the thickness and pH dependent swelling of PEM membranes.[42] Through the Voigt model, the shear, loss, and complex moduli could be calculated and agreed with complimentary techniques.

QCM-D permits the study of proteins under dynamic and static conditions, which is vital to the application to different medical device circumstances. The laminar flow dynamics of the QCM-D flow module were established through computational methods.[44] Laminar flow is a precondition because turbulence without fully

developed flow can induce shear distortion of the crystal's vibrations that may be decoupled from its motion. The Reynolds number (Re) is a dimensionless parameter describing the turbulence of a dynamic fluid, where Re>2000 are turbulent systems. Typical Re from the QCM-D range from 0.2-2 and are lower than typical physiologic conditions in large blood vessels.[45] While the behavior of proteins such as fibrinogen or vWf are known to be shear dependent,[46] the ability to conduct dynamic experiments is still more optimal when a medical device's application involves flowing media.

QCM-D has been used to describe protein adsorption on self-assembled monolayers, BCPs, metals, and biopolymers.[9, 24, 47-50] Reduced protein adsorption under flow has been shown on many surfaces using QCM-D and complimentary techniques.[51-53] The origin of flow reduced adsorption has been hypothesized to occur due to shorter contact times.[51] Since the QCM-D is an acoustic technique, compositional information about adlayers cannot be determined in competitive adsorptions. However, antibodies that bind to proteins within a competitive system can yield information about relative binding and characterize the adlayer's nature.[54]

Qualitative information about the conformation of adsorbed protein layers can be afforded through the analysis of dissipation versus frequency plots (D-f plots).[55] Through these studies, a qualitative relationship between the slope of D-f plots and protein stability against denaturation was established. The increased dissipation of partially denatured adlayers originates from structural transitions from compact folded states to randomly coiled conformations.[55, 56] D-f plots with large slopes may

be indicative of protein denaturation; however complimentary techniques are required to confirm these hypotheses.

1.3.3 Patterning Surfaces

Self-assembling systems are the prevailing technique for fabricating bulk or surface patterns. The top-down approach to self-assembly attempts to strip down larger components by using various stimuli, including milling, lithography, and other variations used mostly in the semiconductor industry. Electron-beam (e-beam) lithography is a high resolution technique with the ability to pattern single nanometers; however e-beam tools require large capital expenditures, making the cost of a silicon master exceedingly high. Whitesides developed soft lithography where masters are fabricated using e-beam lithography and made into reusable stamps for printing.[57] The soft lithography technique was further improved by Desimone and coworkers to create nanoparticles with controlled shape and size using high throughput continuous mold manufacturing processes.[58]

The bottom-up approach to self-assembly uses materials made of smaller individual components to form superstructures through a combination of weak non-covalent interactions such as Van der Waals forces, hydrogen bonding, and ionic bonds.[59] The advantage of the bottom-up approach is the cost effectiveness of self-organizing systems. The bottom-up approach includes protein nanofibers, colloidal assemblies, liposomes, and BCPs, among numerous other systems.[60, 61] The bottom-up approach's strength is the tunable final properties of the assembled construct through intelligent molecular design.[62] This dissertation will focus on synthetic BCPs to create

nanostructured surfaces. The principle reason for using BCPs to form nanostructures is their cost effectiveness and ability to pattern large area films with little material.

1.3.3.1 Block Copolymers

BCPs consist of at least two unique homopolymer sequences covalently bound to one another. BCPs encompass a portion of the bottom-up approach to self-assembly due to their inherent ability to organize into nanostructured materials. The miscibility of two homopolymers within each other is low, which typically results in phase separation when processing homopolymer blends.[63] Two polymers are miscible if the change in Gibbs free energy, ΔG, is negative:

$$\Delta G_{mix} = \Delta H_{mix} - T\Delta S_{mix}$$

The chemical linkage between BCP segments inhibits macrophase separation and results in the microphase separation phenomena when ΔG_{mix} is positive .[63]

Microphase separation in BCPs was predicted by theoretical calculations by Leibler.[64] The BCP phase diagram developed by Leibler's theory dictates that microphase separation occurs above a critical χN value known as the order-disorder transition (ODT). The Flory interaction parameter between the segments of a BCP, χ, can be approximated as:[65]

$$\chi \approx \alpha + \beta T^{-1}$$

Where α and β are experimentally determined enthalpic and enthalpic parameters for a given BCP system and T=temperature

Below the ODT, BCPs exist in a disordered homogeneous state. The ODT is defined by the spinodal line, where χN_S the critical value of χN where the microphase separation phenomena occurs. When $\chi N \approx 10$ for the case of symmetric BCPs, a shift from a homogenous mixtures to microphase separated domains occurs.[64] Mixed BCP domains are typically observed experimentally in low MW systems such as oligomers or with chemically similar blocks with low χ values. Figure 1.4 shows the experimentally determined phase diagram for poly(styrene)-block-poly(isoprene) BCPs and some of the morphologies possible from A-B diblock copolymer systems.

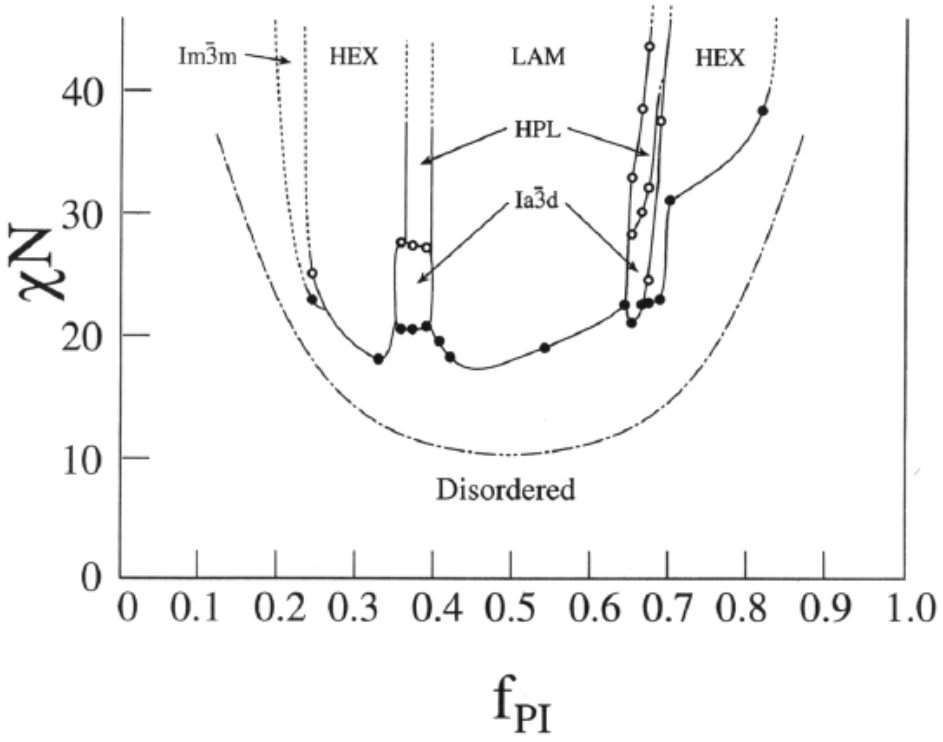

Figure 1.4. Experimentally determined phase diagram for poly(styrene)-block-poly(isoprene) diblock copolymers. (Reproduced from Khandpur et al[66])

BCP morphology depends on both χN and the volume fraction (ϕ) of each respective block as shown in the phase diagram. For an arbitrarily large χN value, lamellae, ordered bicontinuous double-diamond, hexagonal closed packed cylinders, and body centered cubic spherical morphologies can be obtained as ϕ_A shifts from 0.5 to 0.85. Structure within structure morphologies such as spheres within lamellae and sphere, spheres within cylinders, and various other permutations of the basic morphologies are possible when BCPs contain more than two distinct homopolymer sequences.[67] However, this dissertation will focus on the properties of AB diblock or ABA triblock copolymers, which have similar properties to their diblock analogs. Leibler's theory indicates that for $\chi N=20$ and $\phi_A=0.75$, the BCP structure would consist of B-block cylinders within an A-block matrix. For the inverse situation, where $\chi N=20$ and $\phi_A=0.25$, the BCP morphology would consist of A-block cylinders within a B-block matrix. As ϕ_A approaches unity, χN_S diverges towards infinity because the amount of the B-block approaches zero.

BCP systems with large χN values are described with the strongly segregated limit (SSL) of BCP microphase separation.[63] Likewise, small χN values are described by a weakly segregated limit (WSL). WSL BCPs are traditionally defined as systems with $\chi N>>10$, whereas SSL BCPs have $\chi N\leq 10$. The implications of each limit correspond to the sharpness of the phase boundary between adjacent BCP domains. Thus, WSL BCPs have sharp phase boundaries and SSL BCPs contain more diffuse composition transitions. While this dissertation did not experimentally determine χN values of the model system described, there is some evidence in the literature that some amphiphilic BCPs consist of strongly segregated.[68]

Typically, the MW of relative fraction of each segment in a BCP is targeted during the synthetic process. Reaction parameters can be adjusted by a polymer chemist to produce BCPs with desired morphologies and sizes. The prevailing technique for synthesizing BCPs is anionic polymerization.[65] Anionic polymerization is a "living" reaction, where no termination steps exist until the addition of a terminating compound.[69] When monomer initiation is much faster than chain propagation, polymers with narrow MW distributions can be obtained.

Anionic polymerization can obtain polymers with low polydispersity, however this scheme is limited by the lack of reactivity with polar and charged species, such as carboxylic acid groups.[70] A thorough treatment of polymer MW and polydispersity is included later in this text. Protecting groups can be used to synthesize BCPs with charged groups such as the case of poly(styrene)-block-poly(tert-butyl acrylate). After styrene monomer exhaustion during synthesis, the tert-butyl acrylate block is polymerized and subsequently hydrolyzed into poly(acrylic acid) post-polymerization.[71]

One of the primary difficulties with processing BCPs is aligning their domains, which are subject to interfacial effects with the substrate and air during film manufacture. BCP domains can be aligned or oriented by several methods, including but not limited to tuning film thickness, patterned substrates, and external fields.[72] Tuning the film thickness during casting is a simple way to control BCP domain orientation, as validated by both theory and experiments.[73, 74]

Despite the numerous methods to process aligned BCP domains, this dissertation will concentrate on obtaining reasonably oriented films from spin coating. Spin

coating affords high throughput film casting, unlike other processing techniques. Biomedical materials and devices are often fabricated using spray or roll coating with a flash annealing process to dry solvent from the films. These methods are often used for their high throughput; however they require significantly more material than spin coating.

1.3.3.2 Thiol-ene Chemistry

Increasingly, polymers with tailored properties are required for a variety of applications, including surfactants, ionomers, and bioactivity.[75, 76] These polymers are commonly defined as functional polymers, which contain chemical groups that can participate in a reaction or ligand binding without degradation.[77] Functionalities typically exist at the polymer chain end, throughout side chains, or on the branches of dendrimers. End-functional polymers are typically synthesized either by the use of macroinitiators or by chain terminating molecules with an R-group of choice.[78, 79] Dendrimers have been traditionally synthesized by orthogonal coupling reactions, which often require long reaction times.[80] More recently, techniques that involve a modular approach to synthetic chemistry, such as thiol-ene chemistry, were used to rapidly synthesize dendrimers.[81]

A modular synthetic approach is imperative for creating functional polymers for several reasons. Manufacturing costs for monodisperse polymers can be high, thus the ability to create countless materials from one reaction stock would decrease the price of functional polymers. For a reaction to be considered modular, it should efficiently proceed without functional group limitation. Several reaction schemes are modular in

nature, including the Huisgen cycloaddition, Diels-Alder, thiol-yne, and thiol-ene reactions.[82] The thiol-ene reaction is the focus of this dissertation due to the commercial availability of unsaturated BCPs synthesized from diene monomers. Additionally, the PS/PB BCP system used is an analog of the SIBS triblock copolymer used in some blood contacting medical devices.

Alkenes can be modified using several compounds, including but not limited to hydrogen halides, oxymercuration, and catalytic hydrogenation.[83] These reagents are halogenated, toxic, or gaseous, which complicates reaction conditions and waste disposal. Free radical addition, including the thiol-ene reaction, is a method that permits the addition to alkenes without functional group limitations. Sulfur's reactivity with double bonds was discovered in the 19th century by Goodyear to enhance the mechanical integrity of poly(isoprene), or natural rubber.[84] The radically mediated vulcanization technique invented by Goodyear used gaseous sulfur and high temperature to cure rubber. The high temperatures used in vulcanization processes may be incompatible with pharmaceutical compounds. Additionally, the reactivity of unbound sulfur atoms with the disulfide bonds of proteins may cause denaturation.[85] Thus, a synthesis including the removal of unreacted sulfur compounds and processing without high temperatures are optimal for biomaterial coatings.

Thiol-ene reactions involves the addition of functional thiols to unsaturated bonds.[86] These include the crosslinking reaction with multifunctional sulfur compounds, known as vulcanization, and the addition of monofunctional ω–thiols. Recently, thiol-ene chemistry has been explored by several groups to synthesize polymer networks, BCPs, dendrimers, liquid crystals, end-functional and backbone modified polymers.[81,

[87-90] Figure 1.5 schematically depicts some of the modification possibilities with thiol-ene and other modular reaction schemes. These modifications include side groups, chain end, or telechelic functionalities. Thiol-ene chemistry can be employed for interfacial modifications, including solvent dispersed nanoparticles or the surfaces of thin films containing either unsaturated bonds or thiols.[91-93] Photochemical or thermal initiation may be used to generate sulfenyl radicals, although photochemical strategies were found to be more effective.[94] Low intensity ultraviolet sources are capable of generating radicals including renewable resources like sunlight.[95]

After radical initiation, a second initiation step occurs where the radical transfers to the thiol by hydrogen abstraction.[88] The thiol-ene reaction kinetics have been described by several groups and are summarized in Figure 1.6. After thiol addition to

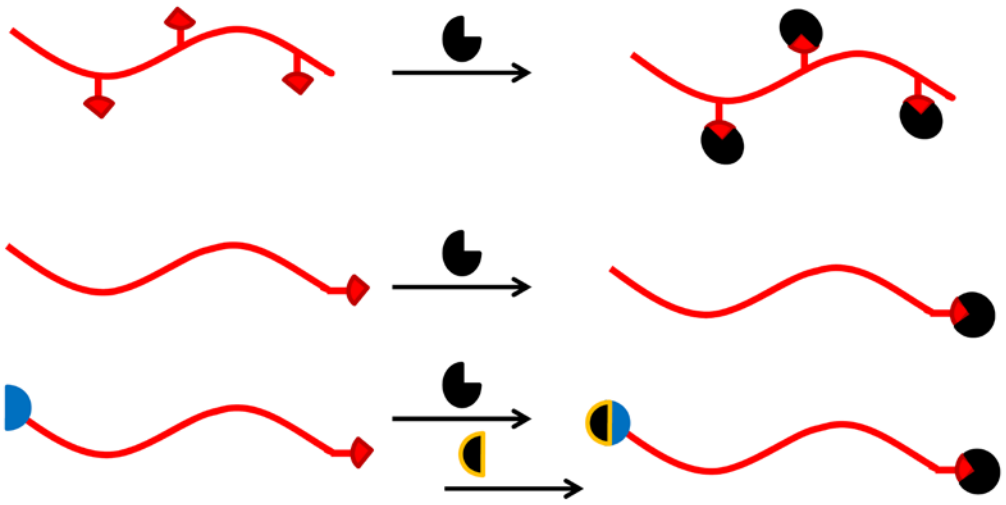

Figure 1.5. Depiction of some modifications possible with thiol-ene chemistry or the combination of two modular processes. These include backbone, end-functional, and telechelic modifications.

an alkene, radical propagation occurs either by initiating another sulfenyl radical or through transfer to the adjacent carbon atom. In the case of the thiol-ene reaction on poly(1,2-butadiene) (PB), radical propagation within the pendant chain can increase the probability of a cyclic reaction occurring, which is discussed later in this section. Termination reactions involve the recombination termination of two sulfenyl radicals, an additional thiol reaction, or reaction with another vinyl group. The latter case is the origin of cyclic group formation in PB.

The thiol-ene reaction on PB is limited by the formation of cyclic groups when intermediate radicals react with adjacent unreacted double bonds. The fate of pendant vinyl groups during and after a thiol-ene reaction are shown schematically in Figure 1.7 for the case PS/PB, such as the polymers synthesized in this dissertation. Possible reaction products are no reaction, thiol addition, and thiol addition followed

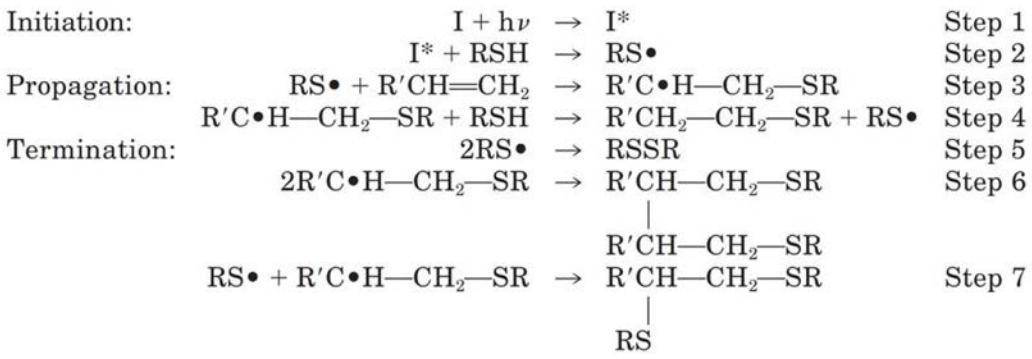

Figure 1.6. Reaction kinetics of the photochemical thiol-ene reaction. A 2-step initiation process results in sulfenyl radical formation. Propagation occurs through radical transfer and termination occurs by recombination. (Reproduced from Cramer et al[88])

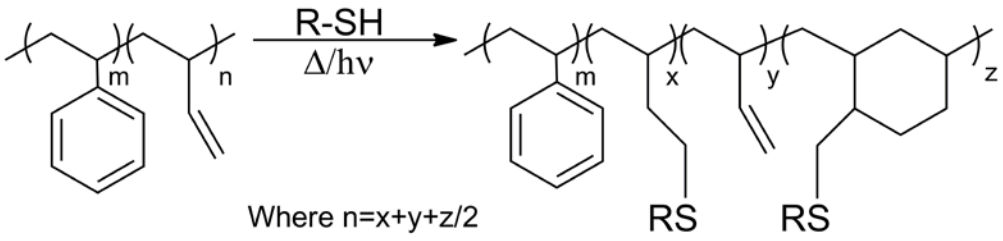

Figure 1.7. Reaction scheme of the thiol-ene reaction on PS/PB block copolymers. Possible reaction routes include thiol addition, no reaction, and cyclic group formation

by cyclic group formation. Although not shown, there is a possibility that the photoinitiator itself adds to the PB side chains; however this side reaction was not observed in any NMR spectra collected throughout this work. Previous studies confirmed that six-membered rings reduce the possible thiol addition yield despite full conversion of double bonds.[96] In spite of cyclic formation in the thiol-ene reaction of PB, high yields were reported in the range of 75% modification, with near quantitative conversion of double bonds in most cases. Some limitations of thiol-ene chemistry were observed by several groups, including reduced efficiency and higher side product formation when using low thiol-ene ratios.[89] Compared to low MW compounds such as monomeric olefins, polymeric starting materials exhibited large decreases in reactivity.[89]

Poly(butadiene) based BCPs are used in this dissertation due to their widespread commercial availability. The diene nature of butadiene monomer feedstocks leads to the formation of both poly(1,4-butadiene) and PB products. Often, a combination of these two similar mers are targeted in the synthesis of poly(butadiene) to inhibit crystallization and maintain elastomeric properties. Previous research confirmed the

pendant vinyl groups of PB were over tenfold more reactive to thiols when compared to the backbone double bonds in poly(1,4-butadiene).[97] The modular capability of thiol-ene chemistry was demonstrated for the synthesis of low MW ionomers without functional group limitations, including alcohols, amines, amino acids, carbohydrates, carboxylic acids, and fluorinated compounds.[75, 76, 96, 98]

The low MW polymer systems previously investigated for the thiol-ene reaction cannot be used for coating applications, which require thin and bulk film processing. Styrene-butadiene BCPs synthesized by numerous manufacturers have MWs in the range of 100-150 kDa, whose mechanical properties and solution viscosity are optimal for film applications. Few studies have examined thiol-ene addition on high MW PB copolymers. Passaglia and Donati found significant issues with crosslinking and low functionalization using thermal initiation on styrene-butadiene random copolymers.[99] In order to decrease crosslinking, lower concentrations of initiator were used at the expense of reduced functionalization. More recently, David and Kornfield were able to graft thiol groups to high hours.[100] These polymers could be further reacted to create functionalities with potential optoelectronic or liquid crystalline properties.

1.4 Analytical Techniques

This section will attempt to concisely discuss the characterization techniques used in this dissertation. Most of this information is available in introductory graduate texts for polymer science and surface analysis; however a thorough background on these techniques would be beneficial to the reader. With that in mind, certain themes will

be emphasized to relate these analytical techniques to the subjects discussed in this text.

1.4.1 Molecular Weight Determination

Polymer MW is defined by several parameters, including the number-average MW (M_n) and the weight average MW (M_w) that are defined as:

$$M_n = \sum n_N M_N$$

$$M_w = \sum w_N M_N$$

Where n_N=number of chains with a degree of polymerization N, M_N=$F_{w\text{-}monomer}$·N, $F_{w\text{-}monomer}$=molar mass of the monomer and w_N=the weight fraction of polymers with N repeat units

The MW of polymers is typically determined by gel permeation chromatography (GPC), also known as size exclusion chromatography.[101] GPC systems consist of a high performance liquid chromatography pump, size exclusive columns, and at least one concentration detector. GPC columns are packed with polymeric beads of defined pore sizes tuned by the manufacturer. During GPC separation, high MW chains can navigate through pore voids and elute in shorter times than low MW analogs. Low MW polymers become entrapped in column pores and require longer elution times than high MW components.

While absolute MWs can be obtained from GPC using a light scattering detector combined with a differential refractive index detector, equivalent values are often calculated due to the wide availability of internal polymer standards made from poly(styrene) (PS), poly(methyl methacrylate) (PMMA), and poly(ethylene oxide) (PEO). A representative GPC result is depicted in Figure 1.8 showing a chromatogram of a PS standard mixture used to relate the elution volume to polymer MW. GPC standards are typically chosen to closely match the repeat mer unit. GPC columns are demarcated with a MW range by their manufacturer. In this region, the relationship between log(MW) versus elution volume is nearly linear.[101] Thus, calibration curves can be obtained using linear regressions to define the equivalent MW of an unknown sample, given that the unknown sample falls within the calibration curve. In this dissertation, PS standards were used due to the styrenic

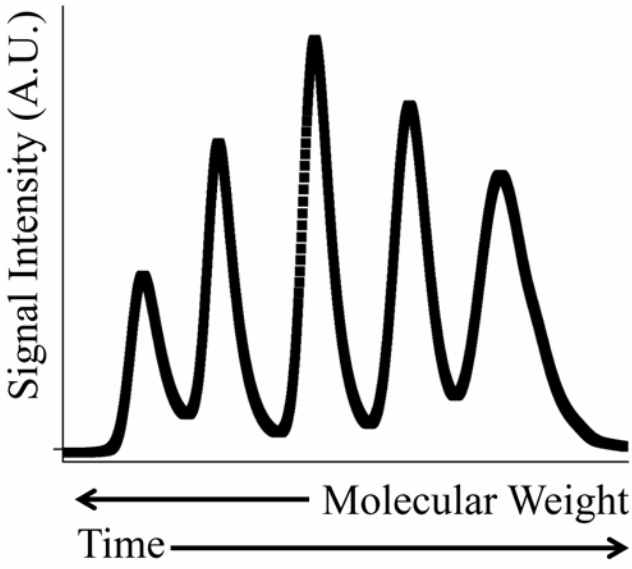

Figure 1.8. Representative GPC chromatogram of narrow molecular weight distribution poly(styrene) standards. Higher molecular weight polymers elute first and are followed by low molecular weight adducts.

nature of the polymers synthesized.

As previously described, polymer MW is defined by several treatments, such as M_n and M_w. The population consistency of polymer MW within a given sample is described as the polydispersity index, PDI, which is defined as:

$$PDI = \frac{M_w}{M_n}$$

Polymers with large PDI are polydisperse and contain a broad MW distribution. For PDI<1.5, these polymers are generally considered monodisperse. The PDI and MW are significant parameters for the polymer chemist because they determine the final properties of a polymer sample. Large PDIs can produce variable mechanical, physical, or solution properties.

1.4.2 Polymer Architecture by Nuclear Magnetic Resonance Spectroscopy

Post synthesis, techniques are required to describe the chain architecture as part of the characterization process. Among the most powerful techniques is nuclear magnetic resonance spectroscopy (NMR). This discussion will be limited to ^{1}H NMR, although the general concepts apply to ^{13}C and ^{19}F NMR. When electromagnetic radiation in the radiofrequency range is applied to nuclei with half integral spin quantum numbers, their magnetic moments align parallel or against the applied field.[102] The radiation frequency required to flip the magnetic moment is defined as the resonance frequency.

Nuclear resonance frequencies in NMR are unique and sensitive to their local environment. Neighboring atoms can shield an atom by resisting its magnetic field and is described as shielding. Electron withdrawing nuclei, such as those with carbonyl bonds, are strongly deshielded. NMR is graphically represented by a dimensionless scale defined as:[102]

$$\delta = \frac{10^6(\nu^{sample} - \nu^{ref})}{\nu^{ref}}$$

Where ν^{sample}=resonance frequency of unknown peak, ν^{ref}=resonance frequency of a known sample

The technique of calibrating to the chemical shift (δ) of a known reference is designed into modern spectrometers. Due to the wide availability of analytical grade deuterated solvents, often they are used as ν^{ref}.

In this dissertation, characterization of the PS/PB starting materials by ^{1}H NMR established the mole fraction of each respective polymer sequence. From these data, experimental recipes for the concentration of thiols were calculated to determine how reaction conditions affected the properties of the final products. After purification and drying, ^{1}H NMR was used to assess whether impurities such as unreacted photoinitiator, monomer, or double bonds existed in the final product. NMR spectra were also used to calculate the addition yield, or functionalization degree of the final products.

1.4.3 Glass Transition Temperature

At the temperature where a melting transition occurs the change in Gibbs free energy, ΔG, is zero, meaning the crystal's free energy is equivalent to that of the melt. In thermodynamic terms, $\frac{\delta G}{\delta T}$ is a discontinuous function at the melting temperature, making it a first order transition.[69] The polymers synthesized in this dissertation are amorphous, meaning they do not form close packed structures such as crystals. While architectural order exists on the polymer chain itself, there are variable free volumes between chains in amorphous polymer films, which inhibit their crystallization. One reason is the inherent polydispersity of polymeric systems due to imperfect reaction kinetics and non-uniform stereochemistry from synthesis, or tacticity. Architectural effects such as branching or side chains also inhibit the crystallization of polymers and thorough treatment is included later in this section.

Despite the lack of crystalline melting, amorphous polymers are temperature responsive at the glass transition. The glass transition temperature, T_g, is typically defined as the onset of segmental mobility in an amorphous polymer system.[69] Segmental mobility is referred as the ability for polymer chains to freely rotate and exchange across one another. At T_g, $\frac{\delta^2 G}{\delta T^2}$ is a discontinuous function, making it a second order phase transition. Physically, there is a discontinuity between the specific volume of polymer chains and their free volumes.

The implications of polymers with T_g above room temperature (RT) is they exist as glassy and sometimes brittle materials. Polymers with T_g below RT are flexible and

easily deformed by mechanical force. The T_g of classical amorphous commodity polymers such as PS, poly(1,4-butadiene), and poly(methyl methacrylate) are approximately 100, -88, and 90 °C, respectivefully.[103] Thus, the measurement of the glass transition can provide qualitative information about a polymer's mechanical properties.

There are numerous architectural factors within a polymer chain that determines its T_g. Since high chain flexibility and rotation is characteristic of polymers above T_g, the primary factor determining T_g is the backbone of the polymer itself. Polymers with aliphatic backbones like poly(ethylene) can freely rotate and have low T_g's in the range of -140 °C after discounting crystallinity.[104] The addition of a backbone aromatic group in the case of poly(p-xylylene) causes an increase of Tg to 80 °C.[105] The aromatic ring in the backbone of poly(p-xylylene) significantly decreases the configurational entropy of the polymer, which requires more energy to induce segmental motion. Configurational entropy can be considered as the permutations where bond rotation in a chain can occur. While not entirely equivalent to poly(p-xylylene), some of the PS/PB BCPs synthesized in this dissertation were subject to increased T_g due to this effect.

Longer side chains off the backbone can also effectively increase a polymer's T_g due to lost free volume.[102] The free volume of a polymer, V_f, is defined as:

$$V_f = V - V_o$$

Where V= sample volume and V_0=the volume occupied by polymer chains

Linear polymers without side chains such as poly(1,4-butadiene) have high free volumes and readily permit the thermal expansion of chains when approaching T_g. Polymers with side chains like PB have lower free volumes and require higher temperatures for segmental motion to begin.

The extent of heterogeneity within a polymer's architecture governs glass transition properties. Discounting crystallinity, homopolymers exhibit a single glass transition due to phase uniformity.[102] Random, alternating, and statistical copolymers also exhibit one glass transition since they form one uniform phase. Beyond the ODT of BCPs, their microphase separation properties induce two distinct glass transitions.

A common method for T_g measurement is the differential scanning calorimeter (DSC).With two heat flow sensors, a reference pan and a container with an unknown sample are subjected to controlled heating ramps. When measuring the thermal properties of a dry polymer in air, the reference pan is empty and eliminates contributions from the DSC pan. While sinusoidal heating and cooling ramps are available from "modulated" DSC (MDSC), the experimental protocols used for this dissertation involve linear heating and cooling ramps. Often MDSC is used for hard to detect transitions, which were not the case for these studies. In the absence of a phase transition, DSC thermograms are relatively linear when plotting heat flow versus temperature. Upon the onset of a phase transition, such as the glass transition, a discontinuity in the thermogram occurs, which is defined as the onset. Using software packages available from vendors such as Perkin-Elmer or TA Instruments,

the onset, midpoint, and completion of the transitions are reported. In this dissertation, the midpoints of the glass transitions are reported.

For simplification, polymers with T_g above RT will be referred to as hard polymers, whereas polymers with T_g below RT are deemed soft polymers. The SIBS triblock copolymer used in some medical devices is identified as a thermoplastic elastomer (TPE), which consists of both hard and soft polymer sequences with two distinct T_g's, as discussed above.[106] At RT, TPE BCPs perform like vulcanized rubbers. The hard PS segments of SIBS act like physical crosslinks and significantly enhance the mechanical properties of the soft elastomeric phase. The utility of TPEs is that unlike vulcanized rubbers, they can be heated above the PS hard block's T_g and processed like a thermoplastic.

Due to the wide availability and applicability of SIBS, SBS, and analogous Kraton-like TPEs, considerable research was undertaken to explain their properties. Some interpenetration of the soft block's chains into the hard PS blocks was hypothesized to be responsible for the decreased PS T_g when comparing to homopolymers. While the polymers synthesized in this dissertation are similar to SIBS/SBS and the like, the properties are slightly different. There is less data on PS/PB than the poly(1,4-butadiene) analogs. However, the glass transition temperature is much higher in PB than poly(1,4-butadiene) and may decrease the amount of interpenetration between BCP domains.

1.4.4 Wetting by Contact Angle Measurement

The surfaces prepared in this dissertation contact aqueous media, which necessitates characterization under these conditions. Surface wettability was previously established to be indicative of protein adsorption behavior.[21] For a solid surface (A) contacting an aqueous environment (B) in a gaseous medium (C) the surface tensions (γ) between each respective phase contribute to surface wettability.[107] assuming an inert air medium in the case of water contact angles on a polymer surface, the contact angle is related to γ of each phase in Young's equation:

$$\gamma_{AB} + \gamma_{BC} \cos\theta_0 = \gamma_{AC}$$

Where θ_0=contact angle, γ_{ij}=surface tension between each interface

The primary reason for measuring water contact angles on the BCP nanopatterns in this dissertation was to provide confirmation that the functional groups grafted to PB were present on the surface. Amphiphilic BCP systems have surfactant-like properties due to both hydrophilic and hydrophobic segments on a chain and often self-assemble into micelles or vesicles when dissolved in organic solvents. The resultant film may not present these groups on the surfaces without consideration of suitable processing solvents.[108]

The water contact angle can also provide insight into protein adsorption behavior by obtaining a measure of a surface's relative hydrophobicity. The chemistry paradigm "like dissolves like" also corresponds to the behavior of proteins on solid surfaces.

Globular proteins with significant hydrophobic cores adsorbed to hydrophobic polymers may rearrange or denature to reveal their hydrophobic motifs to maximize their entropy.

1.4.5 Atomic Force Microscopy

The proliferation of atomic force microscopy (AFM) has enabled scientists and engineers to image the surface of polymers, metals, cells, and proteins. Additionally, AFM confers the ability to make force measurements on these surfaces. The key advantage of AFM is the lack of radiation damage after sample imaging, unlike scanning electron microscopy (SEM). While some damage to samples occurs on a local scale, the areas are insignificant in comparison to the SEM. Advantages do not come without penalties; due to the scanning and vibrational nature of AFM, over-estimation of feature sizes during imaging can be a factor.

AFM in tapping mode works by the vibrational excitation of a cantilever with a laser, often made from silicon. The AFM probe vibrates at a resonance frequency which is related to its flexibility, defined as the spring constant. A piezoelectric scanner moves the AFM probe as it vibrates in a rastering pattern to scan a surface.[109] Through the scanning process, topographical information about a surface is recorded and the operating parameters can be altered in real-time. Height images are pictorially represented by a color scale with a defined vertical distance set by the user. Figure 1.9 shows a prototypical image from a commercial SBS BCP with a height scale of 15 nm. Depending on the tip used, x, y, and z dimensions can be resolved in the single

nanometer range. Recently, advanced operations of AFM under extremely low temperatures enabled the imaging of a single molecule.[110]

In this dissertation, AFM imaging was used to determine the surface morphology of spin-coated BCP films. Initial experiments using AFM were during an iterative approach to obtain phase separated morphologies from the grafted amphiphilic BCPs. Subsequently, AFM imaging was conducted in both air and in phosphate buffered saline to determine how liquids affected the swelling properties of thiol grafted BCP films.

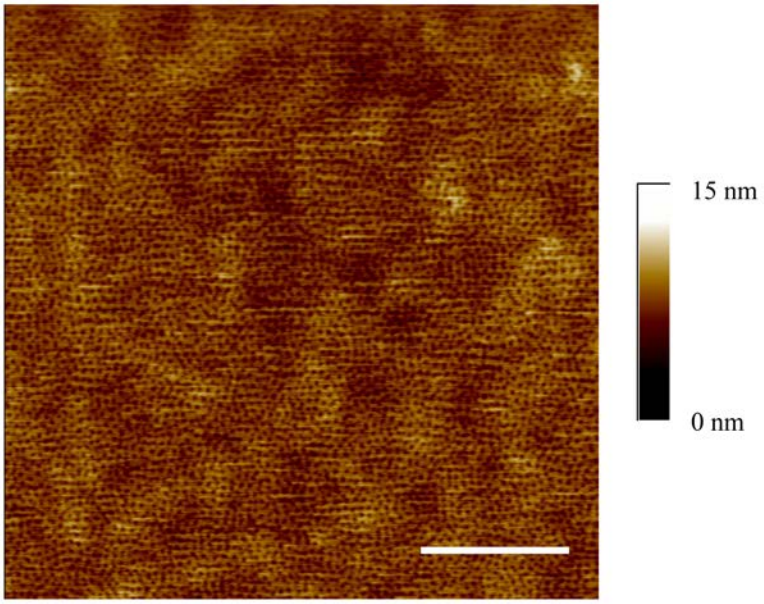

Figure 1.9. Prototypical atomic force micrograph from a commercially available styrene butadiene block copolymer. The colors correspond to the height scale adjacent to the image. Scale bar: 500 nm.

2 : Rapid Modular Thiol-Ene Synthesis and Characterization of Styrene-Butadiene Block Copolymers

In this study, modification of styrene-butadiene block copolymers of varying molecular weight by radical thiol addition is reported using a photochemical strategy that allows for reaction completion within one hour. While alkylation of PB was shown to control the orientation of self-assembled butadiene-ethylene oxide block copolymers,[111] this study seeks to synthesize and process a modular collection of highly functionalized BCP nanostructured films with similar morphologies. Low thiol-ene ratios increased the polydispersity index and in some cases, induced gelation of the modified or "daughter" polymers.

Increased thiol concentrations allowed for efficient grafting of various functional groups, including amines, acids, amides, and a pharmaceutical with a pendant thiol. These polymers were characterized using NMR, GPC, and DSC. Additionally, microphase separation of the modified polymers into nanostructured domains from solution film casting is described and characterized using AFM. This work demonstrates the versatility of the thiol-ene reaction in creating a novel class of patterned block copolymers with tunable chemistry.

2.1 Experimental Section

2.1.1 Materials and Methods

Captopril, thioglycolic acid, boc-cysteamine, thiosalicylic acid, 2-diethylaminoethanethiol hydrochloride (DAET), anhydrous tetrahydrofuran (THF),

phenylbis(2,4,6-trimethylbenzoyl)phosphine oxide (BAPO), propylene glycol monomethyl ether acetate, dimethylformamide, and chloroform were all purchased from Sigma Aldrich (St. Louis, MO) and used as received. Deuterated chloroform and tetrahydrofuran were purchased from Cambridge Isotopes (Andover, MA). EasiVial PS standards for gel permeation chromatography (GPC) calibration were purchased from Agilent Technologies (Santa Clara, CA). Various PS/PB diblock and a poly(styrene)-block-poly(1,2-butadiene)-block-poly(styrene) triblock copolymers were purchased from Polymer Source (Montreal, Canada). The molecular weights and relative molar percentages, as determined by GPC and ^{1}H nuclear magnetic resonance (NMR) spectroscopy, are summarized in Table 2.1.

2.1.2 Synthesis

PS/PB and PS/PB/PS were modified with various thiol compounds radically

Molecular Weight (kDa)[a]	PDI[b]	Mol% PB[c]
8.5-b-8.0	1.08	65
19.3-b-18.9	1.06	65
63.5-b-33.0	1.13	53
14.1-b-67.0-b-24.0	1.13	71

[a] As described by the manufacturer
[b] Determined by GPC
[c] Determined by NMR

Table 2.1. Summary of the poly(styrene)-block-poly(1,2-butadiene) diblock and triblock copolymers used in this study. Mole percentages were used to determine the thiol-ene ratio for reactions.

initiated using BAPO and UV irradiation. The thiol compounds investigated in this study are summarized in Figure 2.1 and include boc-cysteamine, thioglycolic acid, 2-diethylaminoethanethiol, thiosalicylic acid, and captopril. In a typical procedure, 50 mg of each respective block copolymer (BCP), 25 mg of BAPO photoinitiator, and a predefined concentration of thiol were pre-weighed into vials with Teflon septa and purged with nitrogen for 10 minutes. During the purging process, a minimal amount of anhydrous THF was added via syringe, yielding an approximately 5 wt% solution with respect to polymer. Due to the low solubility of captopril and 2-diethylaminoethanethiol hydrochloride (DAET) in THF, a minimal amount of chloroform was used. After purging, the vials were placed into an UltraLum photocrosslinking oven (λ=365 nm) and irradiated for 60 minutes to generate sulfenyl

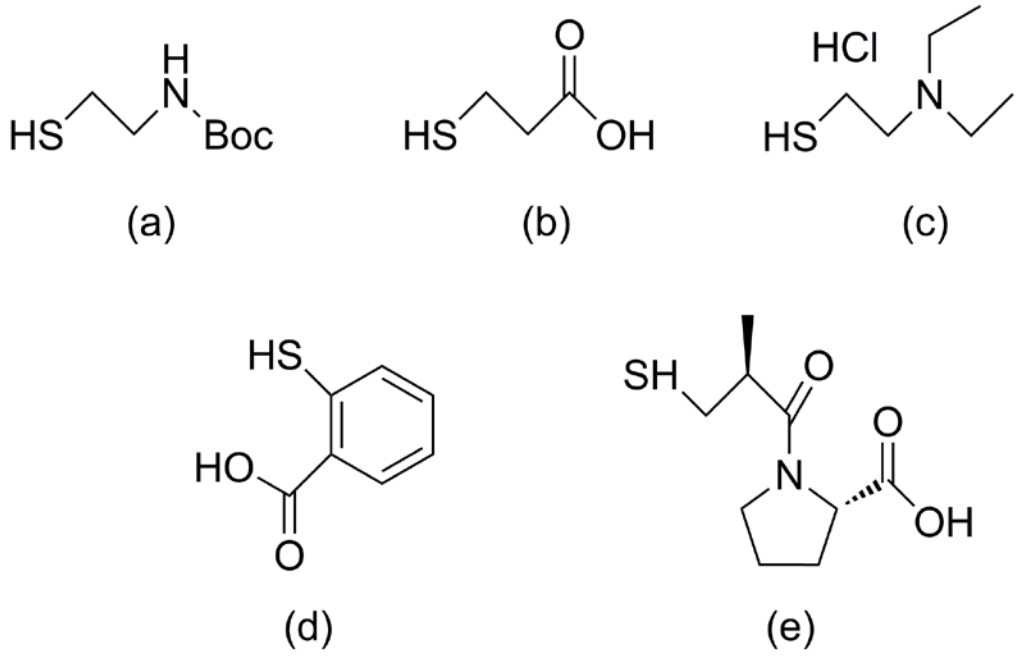

Figure 2.1. Summary of thiols investigated in this study. (a) Boc-cysteamine. (b) Thioglycolic acid. (c) 2-Diethylaminoethanethiol hydrochloride. (d) Thiosalicylic acid. (e) Captopril.

radicals. The distance between the UV lamps and the base of the vials was approximately 15 cm. After UV irradiation, the polymers were concentrated, and precipitated three times in hexane or acetone, followed by redissolution in THF or chloroform each time. Finally, they were dried under vacuum at room temperature until reaching constant mass. It is vital to note that applying heat during vacuum drying often yielded an insoluble product.

For determination of the effects of PB molecular weight on the functionalization and/or gelation of styrene-butadiene BCPs, molar ratios of thiol to double bonds were systematically varied from 1:1 to 10:1. The results reported were calculated from ^{1}H NMR spectra. After recognizing that excess amounts of thiols were required, 10-fold excess of thiol monomers were used to synthesize modified PS/PB block copolymers for calorimetry and thin film analysis.

2.1.3 Characterization

Gel permeation chromatography (GPC) confirmed molecular weight distribution and polydispersity of the stock and modified polymers using a Waters 515 HPLC pump, in-line degasser, Waters 2410 Refractive Index Detector and PolyPore columns in series. PS/PB block copolymers were dissolved at 2 mg/mL in THF. THF was used as the eluent at a flow rate of 1 mL/min and the poly(styrene) equivalent molecular weights reported were determined by constructing a multipoint calibration curve using EasiVial standards (Agilent).

^{1}H NMR spectra were recorded with a Bruker AV-400 high resolution NMR operating at 400 MHz to assess reaction completion. The stock polymers as received

and modified polymers were scanned using deuterated chloroform (d-chloroform), with the exception of the thioglycolic acid and captopril modified polymers, which required the use of deuterated tetrahydrofuran (d-THF). Typically, polymers were dissolved at approximately 2 wt% and scanned 64 times.

Differential scanning calorimetry (DSC) was used to determine the glass transition temperature of the polymers with a TA Instruments Q100 system. The polymers were analyzed using a heat/cool/heat method to erase thermal history with heating rates of 10 °C/min followed by cooling at 5 °C/min. The glass transition temperatures reported are the midpoint of the slope change as determined by the Universal Analysis software package provided by TA Instruments. Prior to conducting DSC measurements, the calorimeter was calibrated with an indium standard.

Block copolymer solutions were prepared at 0.5 wt% and spin coated at 2000 RPM onto silicon wafers with a native oxide layer. Prior to spin coating, silicon wafers were cleaned with isopropyl alcohol, acetone, and dried with a nitrogen stream. Tapping mode atomic force microscopy (AFM) was used to image the surface topography of spin coated block copolymer films using an Asylum MFP-3D system. VistaProbe AFM tips were purchased from Nanoscience Instruments with a nominal tip radius less than 10 nm, spring constant of 48 N/m, and resonant frequency of 190 KHz. 2 x 2 μm scans were completed at 1 Hz with a resolution of 512 x 512 pixels. Image analysis was performed using ImageJ, which is freeware offered by the National Institutes of Health. Average domain sizes were determined in ImageJ with

a minimum of 20 measurements on three different areas and the error reported is the standard error of the mean.

2.2 Results and Discussion

2.2.1 Influence of Molecular Weight on Polydispersity and Functionalization

The molecular weight and polydispersity index (PDI) of the stock polymers, as purchased, are summarized in Table 2.1. NMR integrations were calibrated to the aromatic hydrogens of PS to determine the relative block ratios. The mole percentage of the butadiene block was determined by ^{1}H NMR spectroscopy (NMR) and was further applied to calculate thiol-ene ratios for all subsequently described reactions. The reaction of boc-cysteamine with various butadiene molecular weights was employed as a model reaction to determine the efficiency of the thiol-ene reaction.

BAPO is a cleavage type photoinitiator, whereby UV irradiation causes the formation of a benzoyl and phosphinoyl radical.[112] As discussed in Chapter 1.3.3.2, hydrogen abstraction induces a second initiation step which forms a sulfenyl radical. The sulfenyl radicals attack the double bonds of PB in an anti-Markovnikov fashion. After successful thiol addition, the radical transfers to the adjacent carbon where it may initiate another sulfenyl radical, react with an adjacent mer's pendant vinyl group, or terminate via a recombination termination process. The specifics of thiol-ene reactions on PB using the BAPO photoinitiator are shown schematically in Figure 2.2 for clarification.

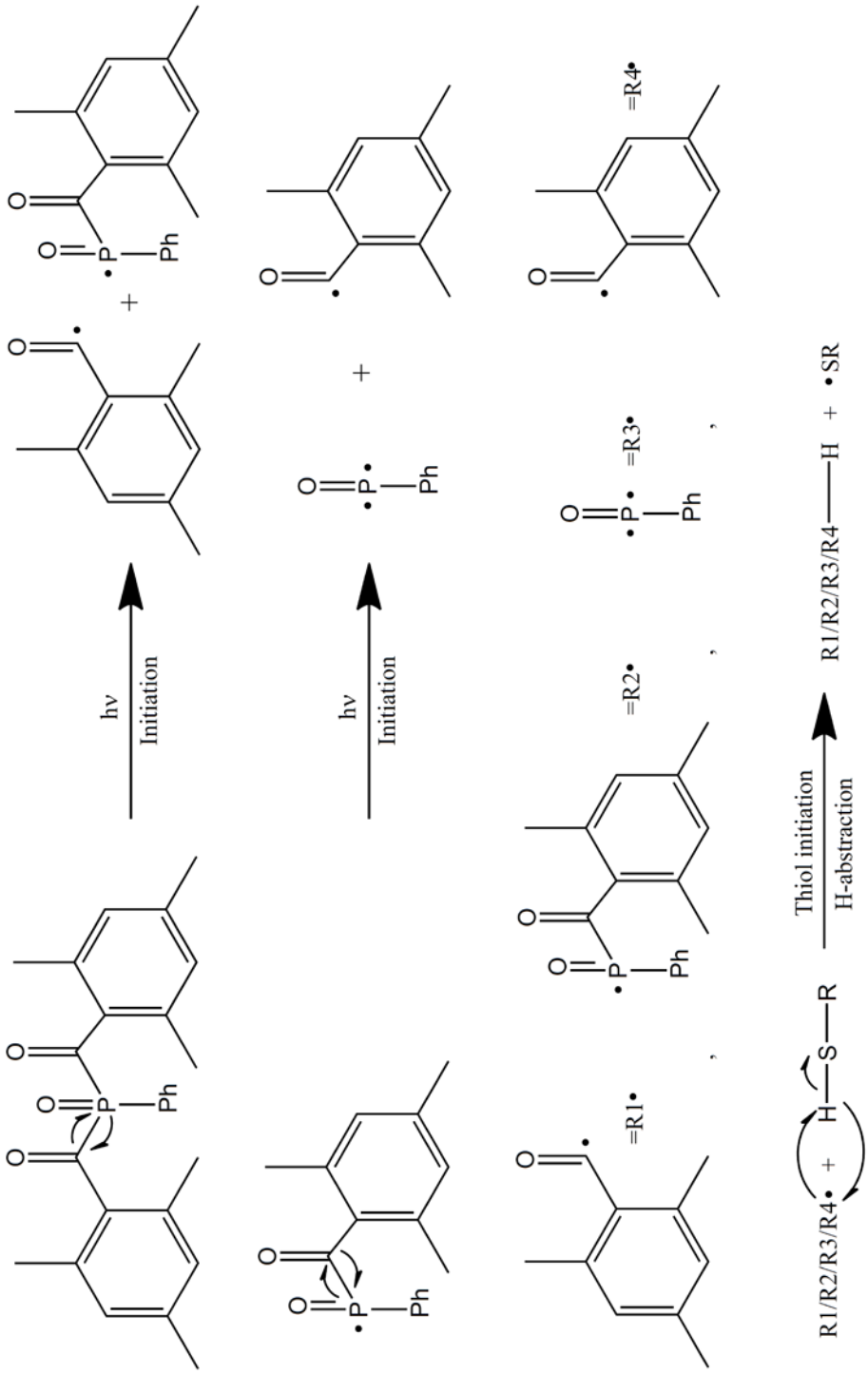

Figure 2.2. Summary of the radical initiation of the BAPO photoinitiator and transfer to thiols by hydrogen abstraction (Adapted from Fisher et al[113])

Radical addition of boc-cysteamine to the pendant vinyl groups of PS/PB block copolymers generally occurred in an efficient manner. Modifications between approximately 50-90% were possible with the lowest molecular weight block copolymer. However, the range of functionalization narrowed to between approximately 70-90% when starting from higher molecular weight parent polymers. Less than quantitative thiol addition derives from the cyclic reaction between active radicals and adjacent, unreacted double bonds. This reaction is confirmed by the lack of remaining double bonds in the modified polymers without quantitative thiol addition. The cyclic reaction is unique to the thiol-ene reaction of PB and is thoroughly discussed in literature.[98]

After UV irradiation, several of the higher molecular weight polymer products showed visible viscosity increases. Despite the solubility of reaction stocks from equimolar concentrations of thiol and vinyl groups during purification, some of these polymers formed an insoluble gel with the exception of the lowest two molecular weight PS/PB polymers. Thus, determinations of the PDI and functionalization degree were not possible for these polymers and are described in Table 2.2 as “gel”. GPC determination for the 8.5-b-8.0 and 19.3-b-18.9 kDa with equimolar thiol-ene concentrations show slight PDI increases on the order of 0.2-0.3 compared to their parent polymers. The PDI of polymer products generally decreases when higher excess of thiol are applied in the polymer modifications, regardless of molecular weight. Specifically, a tenfold excess of boc-cysteamine increased the PDIs of daughter polymer by approximately 0.1, when compared to the high molecular weight parent polymer. In contrast, equimolar and five-fold excess concentrations of thiol led

Molecular Weight (kDa)	Thiol:ene	PDI[a]	f ± SEM (%)[b]
8.5-b-8	Stock	1.08	N/A
	1	1.45	51 ± 1
	5	1.19	70 ± 3
	10	1.12	87 ± 3
19.3-b-18.9	Stock	1.06	N/A
	1	1.23	58 ± 2
	5	1.20	82 ± 2
	10	1.16	93 ± 3
63.3-b-33	Stock	1.13	N/A
	1	Gel	Gel
	5	1.32	70 ± 2
	10	1.25	79 ± 1
14.1-b-67-b-24	Stock	1.13	N/A
	1	Gel	Gel
	5	1.41	83 ± 2
	10	1.28	88 ± 2

[a] Determined by GPC

[b] Determined by NMR

Table 2.2. Effects of boc-cysteamine concentration on the polydispersity index and functionalization degree

to gelation or a 1.41 PDI, respectively. This indicated that the PDI of modified polymers increased due to low thiol-ene ratios; when using equimolar concentrations, this induced gelation of the daughter polymers.

As shown in Table 2.2, the functionalization degree increased with higher thiol-ene ratios and saturated near 90% for the lowest molecular weight polymer. As the molecular weight of the polymers increased, the efficiency of the thiol-ene reaction slightly decreased and resulted in modifications around 80%. Despite the ability to control functionalization on low molecular weight PS/PB block copolymers, low thiol-ene ratios generally increased the PDI of high molecular weight polymers and in some cases induced gelation. Additionally, the potential range of functionalization was narrowed with high molecular weight BCPs. Assuming that all chains within a relatively monodisperse polymer solution have equal reactivity towards thiols, the PDI increase suggests a low density of crosslinks.

Radicals remain active after thiol addition and there are several possibilities for their fate. The active radical can undergo chain transfer and initiate another sulfenyl radical.[89] Radicals can also react with adjacent and unreacted double bonds to form cyclic groups.[96] Finally, two radicals can terminate through recombination and result in intrachain or interchain crosslinking.[89] A combination of these processes may occur; however, recombination termination is most likely the culprit in increased PDIs and gelation products since neither chain transfer nor cyclic group formation would result in gelation.

The observed results from PS/PB modification at low thiol-ene ratios with different molecular weights are supported by theory, where the critical cross-link density for

gelation scales inversely with the degree of polymerization (DP).[103] Thus, higher molecular weight polymers are more susceptible to forming infinite networks. The DP of the butadiene block of the BCPs investigated range from approximately 150-1240 repeat units. The critical crosslink densities for these molecular weights are approximately 0.6% and 0.08% of mer units, respectively. For the highest molecular weight polymer, this corresponds approximately to one crosslinked mer unit per one thousand inducing gelation. These theoretical numbers support the observed experimental results in Table 2.2, which shows that higher molecular weight polymers have a higher propensity for gel formation.

When the thiol-ene ratio was systematically increased, a trend of decreased polydispersity was observed. The chromatogram for the triblock copolymer and the daughter polymer with a tenfold excess of boc-cysteamine is shown in Figure 2.3. The chromatogram shows a modest shift in the peak elution volume towards a higher molecular weight range when comparing the modified polymer to that of the stock. Additionally, a similar narrow molecular weight distribution is conserved between the stock and modified polymers. Various applications, including those for biomedical devices, require materials that can withstand cyclical loading. High molecular weight polymers are typically used for coatings due to their advantageous mechanical properties. The experimental observations indicate a large excess of thiol is required to maintain narrow PS/PB molecular weight distribution and inhibit gelation. While lower degrees of functionality were not presented in this study, perhaps the use of thiolated alkanes as co-monomers may allow for modifications of PS/PB BCPs on the

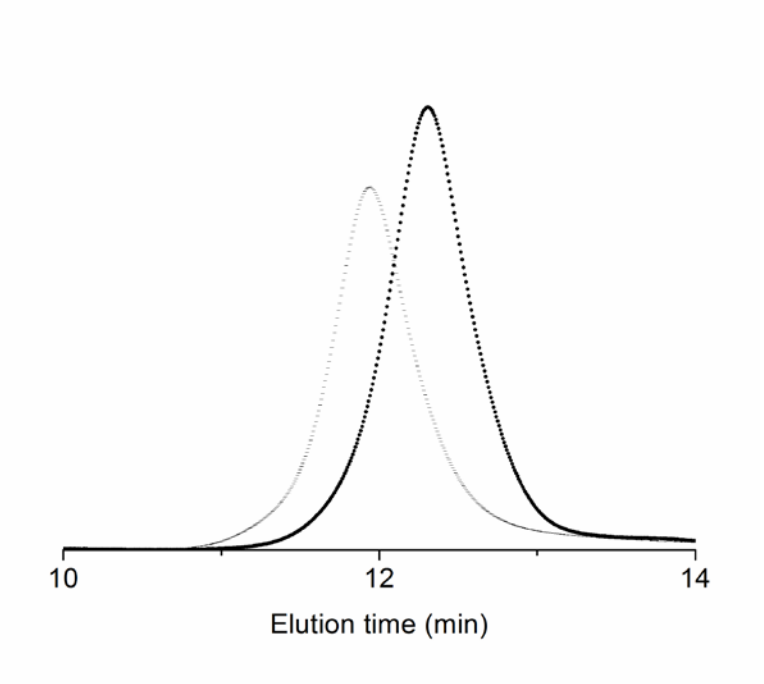

Figure 2.3. Gel permeation chromatography of 14.1 kDa-b-67.0 kDa-b-24.0 kDa PS/PB/PS triblock copolymer and another modified with a 10:1 thiol-ene ratio of boc-cysteamine. (Stock: dark dots, Modified: light dashes).

order of 20-70%. Despite these issues, the photoinitiated thiol-ene reaction presents an effective and facile route for rapid functionalization of butadiene BCPs.

2.2.2 Synthesis of Functional Block Copolymers

After investigating the molecular weight effects of thiol addition, block copolymers were synthesized with a wide set of functionalities. The monomers used in this study were boc-cysteamine, thioglycolic acid, thiosalicylic acid, captopril, and 2-diethylaminoethanethiol hydrochloride (DAET), whose structures are depicted in Figure 2.1. Modified polymers were easily produced and obtained in yields of ~70%, with the exception of thiosalicyclic acid. The PS/PB BCPs reacted with thiosalicylic

acid contained a similar amount of vinyl groups as the parent polymer. Thus, thiol addition did not occur and was confirmed by NMR. The steric constraints from the carboxylic acid group ortho to the thiol group may inhibit thiosalicyclic acid's reactivity with the pendant vinyl groups on PB.[114]

The results from the reaction of the 63.5-block-33.0 kDa stock BCP with various thiolated monomers are described in Table 2.3. The NMR spectra of the unmodified PS/PB BCP as received from Polymer Source is depicted in Figure 2.4 with a summary of the chemical shifts included in Table 2.4. The molar ratio of butadiene to styrene was calculated from the NMR spectra and determined to be 53% PB, or 1.13 PB protons for every PS proton. The NMR spectra and peak assignments are shown for the PS/PB polymers modified with boc-cysteamine, thioglycolic acid, 2-diethylaminoethanethiol, and captopril in Figure 2.4-Figure 2.8 and Table 2.4-Table 2.8 respectively. Similar to previous studies, wide functional group tolerance was

Monomer	Thiol:ene	f ± SEM (%)[a]
Boc-cysteamine	10	79 ± 1
Thioglycolic Acid	10	78 ± 3
2-(Diethylaminoethanethiol) hydrochloride	10	93 ± 2
Captopril	10	69 ± 3
Thiosalicyclic Acid	10	0

[a] Determined by NMR

Table 2.3. Functionalization degree of 63.5 kDa-b-33.0 kDa PS/PB polymers modified using 10:1 thiol-ene ratios on the monomers studied.

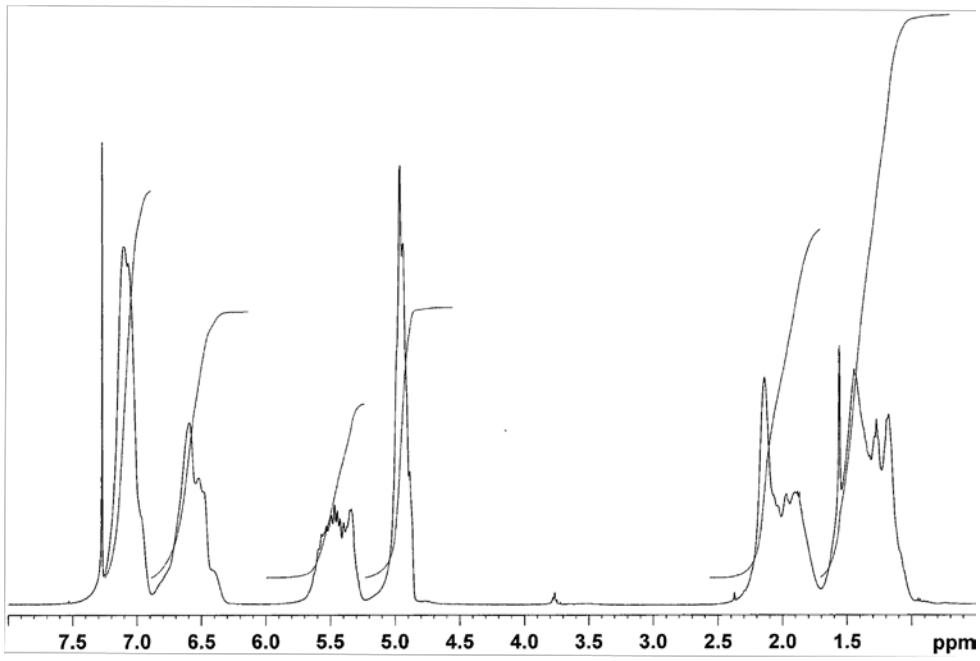

Figure 2.4. ^{1}H NMR spectra of poly(styrene)-block-poly(1,2-butadiene) block copolymer as purchased from the manufacturer.

Shift (ppm)	Bond	# Protons
δ 1.0-2.4	Aliphatic	6H
δ 4.8-5.2	**CH_2**=CH	2H
δ 5.3-5.7	**CH**=CH_2	1H
δ 6.3-6.9	Phenyl	2H
δ 6.9-7.4	Phenyl	3H

Table 2.4. NMR peak assignments of poly(styrene)-block-poly(1,2-butadiene) block copolymer as purchased

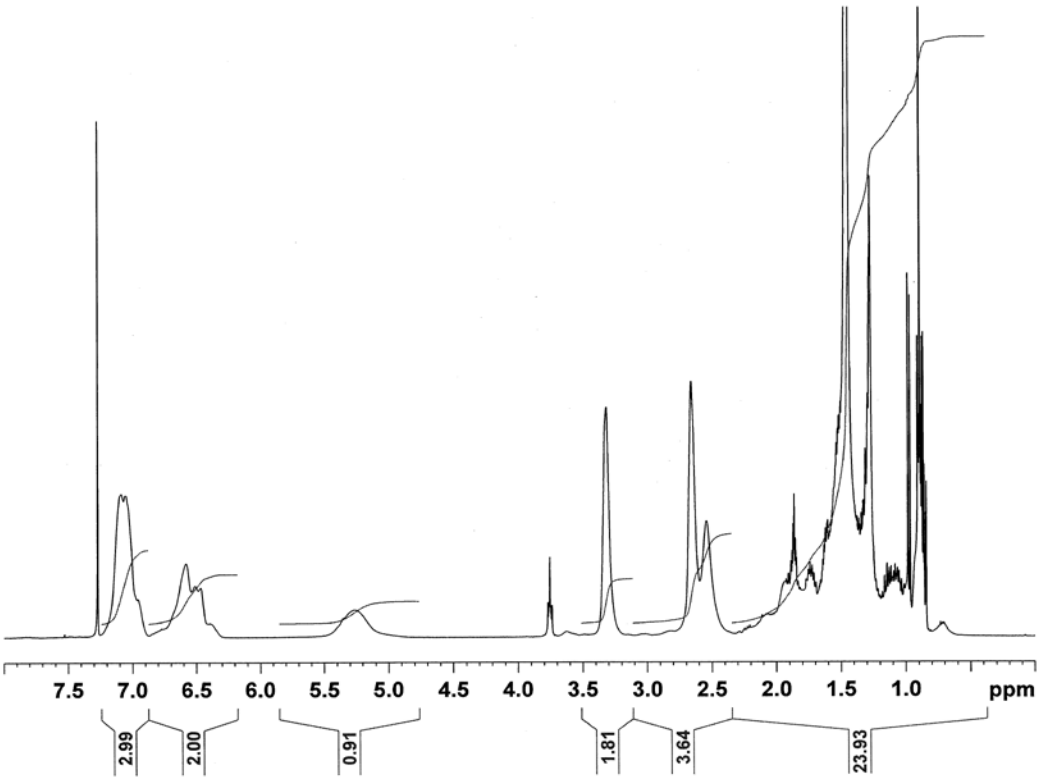

Figure 2.5. ^{1}H NMR spectra of poly(styrene)-block-poly(1,2-butadiene) block copolymer modified with boc-cysteamine

Shift (ppm)	Bond	# Protons
δ 0.8-1	t-butyl	9H
δ 1.2-2.2	Aliphatic	4H
δ 2.4-2.8	CH_2-S-CH_2	4H
δ 3.3-3.4	CH_2-NH	2H
δ 4.7-5.5	NH	1H
δ 6.3-6.9	Phenyl	2H
δ 6.9-7.4	Phenyl	3H

Table 2.5. NMR peak assignments of poly(styrene)-block-poly(1,2-butadiene) block copolymer modified with boc-cysteamine

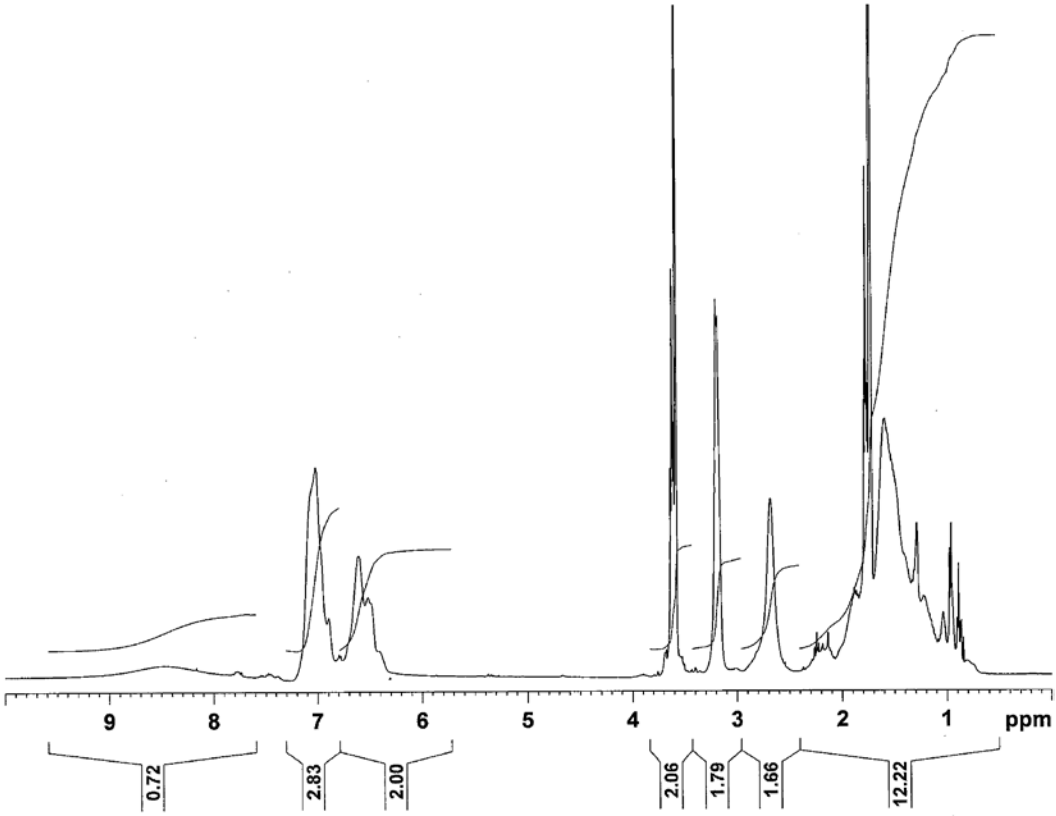

Figure 2.6. ^{1}H NMR spectra of poly(styrene)-block-poly(1,2-butadiene) block copolymer modified with thioglycolic acid

Shift (ppm)	Bond	# Protons
δ 0.8-2.3	Aliphatic	7H
δ 2.5-2.9	CH_2-S	2H
δ 3.1-3.3	S-CH_2-COOH	2H
δ 6.3-6.7	Phenyl	2H
δ 6.8-7.2	Phenyl	3H
δ 7.9-9.2	COOH	1H

Table 2.6. NMR peak assignments of poly(styrene)-block-poly(1,2-butadiene) block copolymer modified with thioglycolic acid

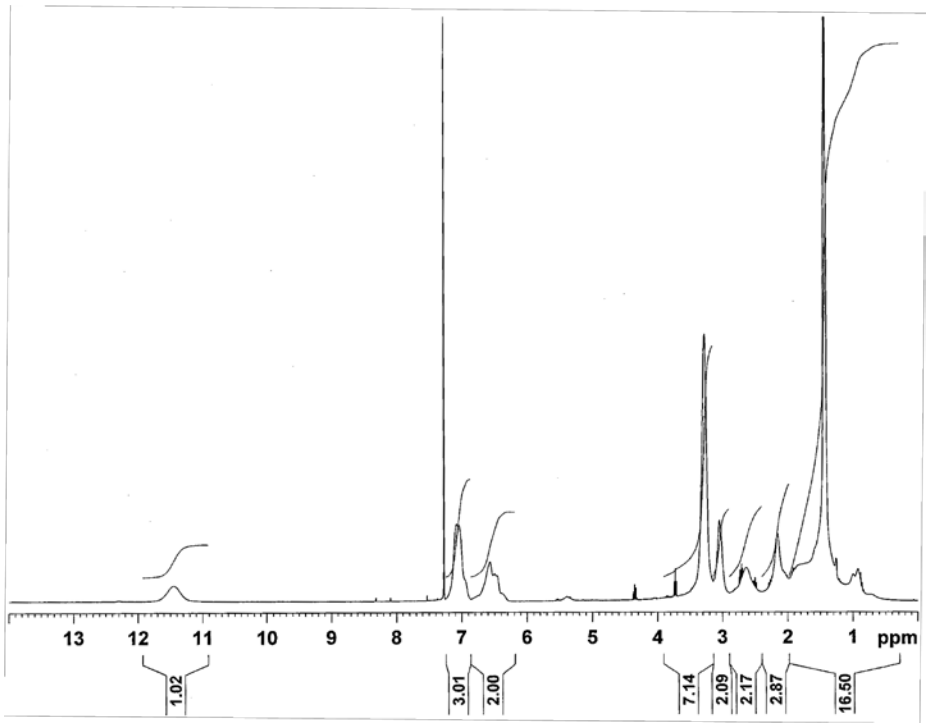

Figure 2.7. ^{1}H NMR spectra of poly(styrene)-block-poly(1,2-butadiene) block copolymer modified with 2-diethylaminoethanethiol hydrochloride.

Shift (ppm)	Bond	# Protons
δ 0.8-2.2	Aliphatic	12H
δ 2.6-2.8	CH_2-S	2H
δ 2.9-3.1	N-CH_2-CH_2	2H
δ 3.2-3.5	$(CH_2)_3$N	6H
δ 6.3-6.8	Phenyl	3H
δ 6.9-7.3	Phenyl	2H
δ 11.2-11.8	HCl	1H

Table 2.7. NMR peak assignments of poly(styrene)-block-poly(1,2-butadiene) block copolymer modified with 2-diethylaminoethanethiol hydrochloride

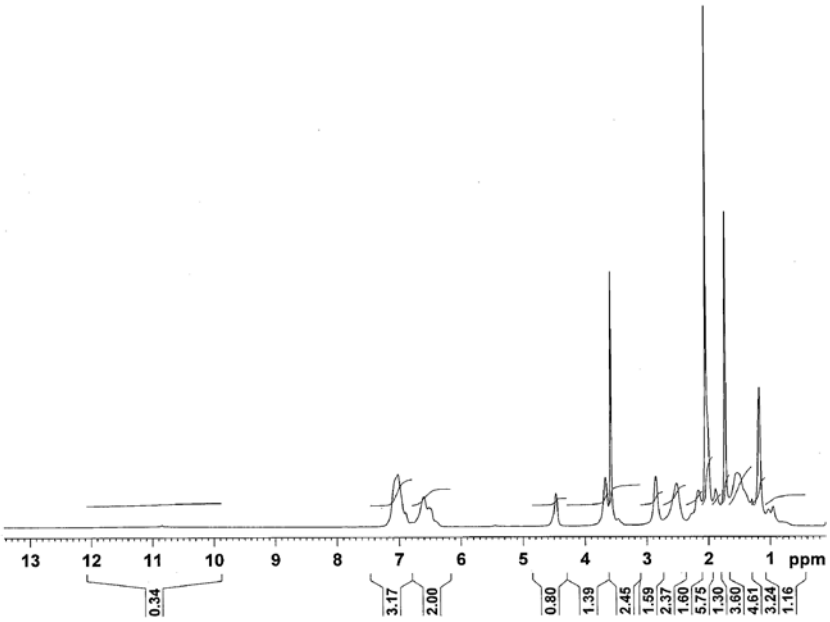

Figure 2.8. ^{1}H NMR spectra of poly(styrene)-block-poly(1,2-butadiene) block copolymer modified with captopril

Shift (ppm)	Bond	# Protons
δ 0.8-2.1	Aliphatic	10H
δ 2.1-2.4	CH_2SH	2H
δ 2.4-2.7	CH_3-CH-C=O	3H
δ 2.8-3.0	S-CH_2-CH_2-C=O	2H
δ 3.6-3.8	CH_2-N	2H
δ 4.4-4.6	N-CH	1H
δ 6.3-6.9	Phenyl	2H
δ 6.9-7.4	Phenyl	3H
δ 10.9	COOH	1H

Table 2.8. NMR peak assignments of poly(styrene)-block-poly(1,2-butadiene) block copolymer modified with captopril

observed using a photochemical strategy for grafting various groups onto PS/PB block copolymers. With the exception of thiosalicylic acid, PS/PB BCPs thiol addition yields were obtained in the range of 70-90%. Despite variable functionalizations, all products show full conversion of vinyl groups between 4.9-5.7 ppm in NMR spectra.

The lowest yield was 69 ± 3% from captopril. As the bulkiness of the group increased, such as with captopril, the functionalization degree decreased. The experimental conditions approach the solubility limit of captopril, thus steric hindrance cannot be explicitly confirmed as the cause of reduced functionalization. However, experiments completed on low MW PB demonstrated that larger R groups resulted in lower modification degrees, despite full conversion of double bonds.[95] Due to the cyclic reaction between active radicals on the PB backbone and adjacent, unreacted double bonds, less than quantitative addition occurred. The appearance of a broad peak at 2.5-2.7 ppm, corresponding to the four protons at the thioether linkage shows the successful addition of thiols to the polymer side chains.

2.2.3 Thermal Characterization

Maintenance of elastomeric behavior is a vital property of styrene-butadiene block copolymers, which are used in a variety of applications, ranging from tires to biomedical devices. The glass transition temperature (T_g) is a key material property to determine whether a polymer conforms to the requirements of a thermoplastic elastomer. Using a heat/cool/heat method to erase thermal history, the T_g's reported are from the PB block only, since the PS T_g remained unmodified during the thiol-ene

reactions. The results from the second DSC heating cycle are shown in Figure 2.9. The glass transition temperature of the PS/PB parent polymer, 63 kDa-block-33.5 kDa, was determined to be -16 °C. The daughter polymers' T_g's increased between 30-60 °C, depending on the specific monomer modification. The glass transition temperatures for the polymers modified with boc-cysteamine, thioglycolic acid, DAET, and captopril were determined to be 15, 33, 43, and 46 °C, respectively.

Large increases in the T_g of the daughter polymers may occur due to several reasons. The dominant driving force for increased T_g may result from the cyclic

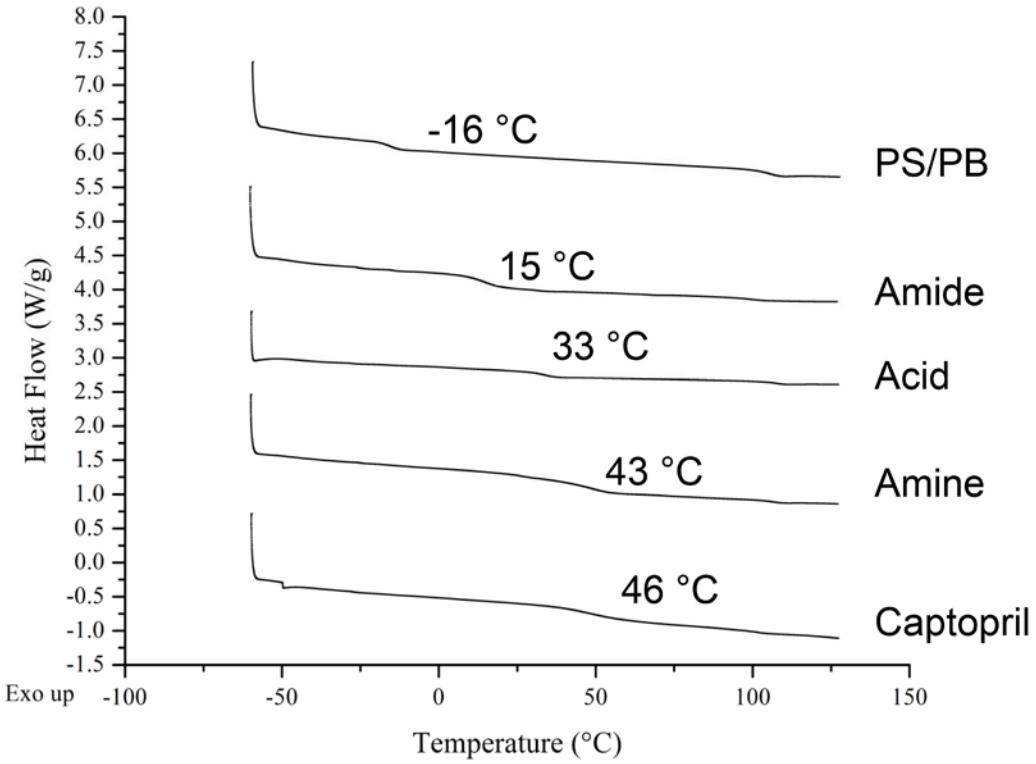

Figure 2.9. Differential scanning calorimetry of monomer dependency of glass transition temperature of functionalized block copolymers using a thiol−ene ratio of 10:1 on PS/PB with a molecular weight of 63.5 kDa-b-33.0 kDa

reaction that exhausted the double bonds unreactive to thiols. As discussed in Chapter 1.4.3, cyclic groups within the backbone of a polymer increase T_g due to lower configurational entropy than linear analogs. [115] In layman terms, the number of potential arrangements by which chains could freely rotate around one another was deceased by the formation of cyclic groups within the polymer backbone.

Another potential mechanism for increased T_g derives from the lost free volume caused by the longer side chains after thiol grafting. Assuming that a polymer's density is constant throughout the modification process, the volume occupied by polymer chains may have increased significantly. Since the free volume is the difference between the volume of a polymer sample and the volume occupied by its chains, less free volume is present to permit the thermal expansion of the polymers during heating. Thus, more energy or higher temperature is required for the onset of segmental motion.

The introduction of polar or charged groups into the side chains may be another compounding factor in the increased T_g after thiol addition. The R groups used for the aforementioned grafting reactions all contain nitrogen and oxygen, which can form hydrogen bonds either within single or between distinct chains. In fact, the lost free volume from increased side chains may increase the probability of hydrogen bonding between distinct chains.

2.2.4 Thin Film Processing

After NMR, GPC, and DSC characterization, optimal conditions for processing the grafted block copolymers were determined. Common solvents used for PS/PB BCPs

such as chlorinated solvents, tetrahydrofuran, and toluene yielded opaque solutions or dispersions which suggested micellar self-assembly. Dynamic light scattering analysis (DLS) indicated the formation of sub-micron particles and was confirmed by film spin coating and AFM analysis.

Various solvents were used to process nanopatterns from each daughter polymer. Generally, the daughter polymers exhibited solubility in dimethylformamide (DMF), propylene glycol monomethyl ether acetate (PGMEA) or dimethyl sulfoxide (DMSO) yet were insoluble in water. Thin films were spin coated from low humidity conditions (<40% RH) from a 0.5% solution at 2000 RPM. The stock 63-block-33 kDa PS/PB diblock copolymer was processed from dichloroethane and formed disordered cylindrical nanostructures after spin coating. Both parallel and perpendicular cylindrical domains existed at the surface from AFM measurements.

Typical results for AFM images are shown in Figure 2.10**.** The average center to center distance of the stock polymer microstructures was determined to be 65.7 ± 1.5 nm. An iterative method was used to process similar nanopatterns from each daughter polymer using the solvents resulting in optically clear solutions, which were typically DMF, PGMEA or DMSO. The boiling point of DMSO was too high for evaporation to occur during spin coating, even after longer times. The center to center domain sizes are tabulated in Table 2.9. Spin coating yielded cylindrical microstructures from the boc-cysteamine, thioglycolic acid, and captopril modified polymers with center to center domain sizes of 66.3 ± 1.5, 74.1 ± 1.9, and 74.5 ± 2.13 nm, respectively. The captopril modified polymer required the addition of approximately 25% (v/v) THF

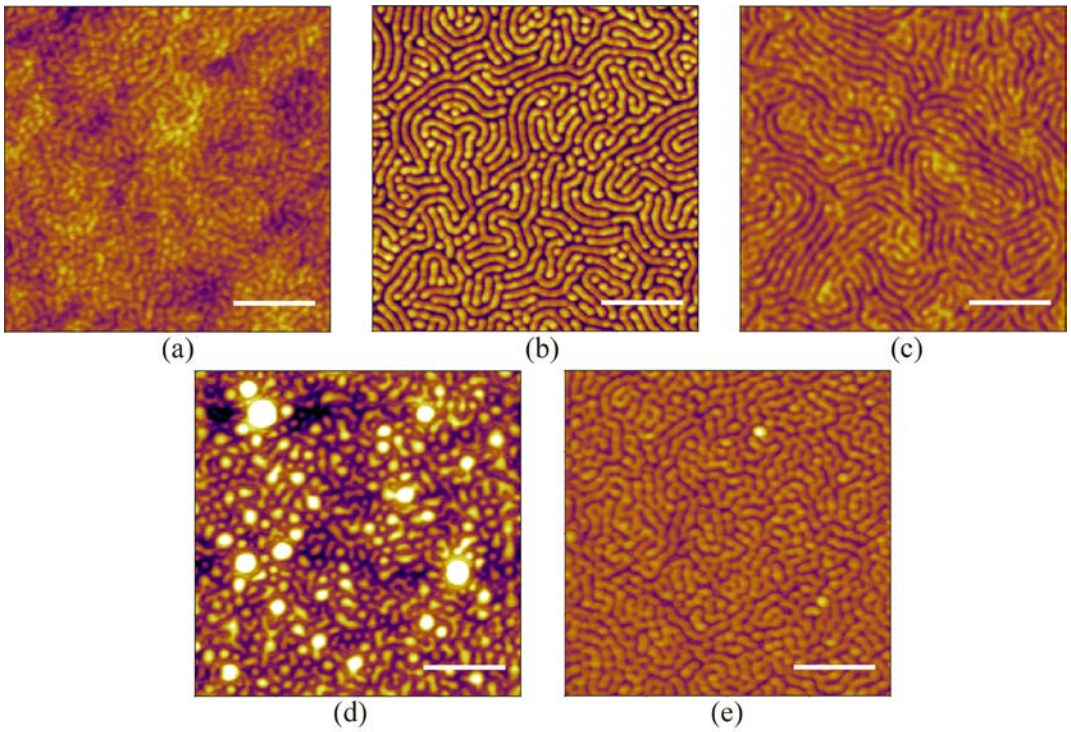

Figure 2.10. Atomic force micrographs of 63 kDa-block-33.5 kDa stock and modified PS/PB block copolymers: (a) parent polymer, as received; (b) boc-cysteamine; (c) thioglycolic acid; (d) 2-(diethylamino)ethanethiol hydrochloride; e) captopril. Scale bars: 500 nm.

for solubility in PGMEA. The DAET modified polymer was spin coated from PGMEA/DMF (90/10 v/v%) due to insolubility in pure PGMEA. The center to center domain sizes of the DAET modified polymer were 80.72 ± 2.72 nm.

DLS showed monodisperse micelles on the order of 20-40 nm for the polymers in PGMEA (not shown). However, the resultant films from spin coating displayed structures typical of microphase separated BCPs and not spherical micelle templates.

Monomer	Center to center spacing ± SEM (nm)
Stock	65.7 ± 1.5
Boc-cysteamine	66.3 ± 1.5
Thioglycolic acid	74.1 ± 1.9
2-(Diethylaminoethanethiol) hydrochloride	80.7 ± 2.7
Captopril	74.5 ± 2.1

Table 2.9. Domain size summary of 63-block-33.5 kDa stock and modified PS/PB block copolymers. The results were calculated from AFM images.

The majority solvent used for spin coating solutions was PGMEA, which has a boiling point of 145°C according to Sigma Aldrich. The T_g of the grafted PS/PB BCPs was demonstrated to range from 15-46 °C in the previous section. Additionally, the T_g of PS is approximately 105 °C, as discussed in Chapter 1.4.3.

Spin casting is a processing method where rapid solvent evaporation can form uniform films. Due to the nature of spin coating, the structures obtained using this processing method are kinetically trapped configurations and not the equilibrium morphologies discussed in Chapter 1.3.3.1.[116] Since the boiling point of PGMEA is much higher than the T_g of both the PB-grafted and PS segments, both blocks undergo their glass transition before solvent evaporation is complete. Despite the T_g of the boc-cysteamine modified polymer being slightly below room temperature, evaporative cooling may induce its glass transition during the spinning process. The remaining grafted PS/PB BCPs have T_g's above room temperature and exist as glasses under ambient conditions.

PGMEA was suggested as a good solvent for aromatic polymers and a poor solvent for charged polymers, in the case of poly(2-vinylnapthalene)-block-poly(acrylic acid).[117] In this particular case, micellar self-assembly was confirmed by small angle scattering, yet microphase separation occurred after spin coating. Sequential vitrification of the BCP blocks during spin coating may induce microphase separation in the resultant films. By this mechanism, micelle cores could first vitrify and provide a template for obtaining reasonably ordered BCP surfaces from merely spin coating.

Despite the high modification degree of the daughter polymers, there was no visible shift into the lamellar region for symmetric block copolymers. This may be due to the micellar template from solution. Seemingly, as the functionalization degree increased, the level of parallel cylindrical domain formation also increased, most notably in the boc-cysteamine modified BCP films. The parallel orientation of quasi-cylindrical domains is in agreement with studies detailing alkylation of PB side chains.[111] An additional factor in parallel domain orientation may be due to the nature of thin films. When film thicknesses are less than the equilibrium domain size of the block copolymers, parallel domains can form, as validated by theory and experimental data in other systems.[73]

2.3 Conclusion

We have described a photochemical thiol-ene strategy for creating a versatile set of functional styrene-butadiene block copolymers. The polymers synthesized and characterized confer the ability to control chemistry at the nanoscale and contain precursors that are readily available as commodity polymers. Amine, carboxylic acid, amide, and pharmaceutical compounds were successfully grafted onto the block

copolymers in reasonable yields. Although the polydispersity index increased with higher molecular weight polymers, high grafting yields were possible with excess thiol.

These novel functional block copolymers maintained glass transition temperatures near or below room temperature, allowing for their application as elastomeric materials. Despite the amphoteric nature of the daughter polymers, microphase separation of the individual polymer blocks was observed when the casting solvent used was polar with a high boiling point. The highly functional polymers described can be used to make modular nanopatterns.

3 Protein Adsorption on Block Copolymer Nanopatterns

In this study, the model system synthesized in Chapter 2 was further characterized using contact angle measurement and atomic force microscopy (AFM). A quartz crystal microbalance with dissipation monitoring (QCM-D) was used to measure the adsorption of proteins with distinct size, charge, and rigidity under both dynamic and static conditions. The wettability of the BCP surface patterns was significantly increased by thiol grafting, and AFM imaging suggested this originated from selective block swelling of charged BCP domains. Protein adsorption measurements by QCM-D confirmed that both the BCP nanopatterns and protein characteristics strongly influence the nature of adlayers. Disproportionate increase in protein adsorption under flow was observed for many nanopatterned surfaces containing polyelectrolyte moieties compared to experiments performed under static conditions.

3.1 Experimental Section

3.1.1 Materials and methods

Poly(styrene)-block-(1,2-butadiene) (PS/PB) BCPs were purchased from Polymer Source (Montreal, Canada). Untreated poly(styrene) (PS) petri dishes, 30% ammonium hydroxide (NH_4OH), tetrahydrofuran (THF), and dimethyl formamide (DMF) were purchased from Fisher Scientific (Pittsburgh, PA). Poly(ethylene-co-acrylic acid) (PEAA) was purchased from Allied Signal Advanced Materials (Sunnydale, CA). 1X phosphate buffered saline pH 7.4 (PBS), 30% hydrogen peroxide (H_2O_2), sodium dodecyl sulfate (SDS), propylene glycol monomethyl ether

acetate, immunoglobulin g (IgG) (human serum, 95%), bovine serum albumin (BSA) (protease free, 99%), cytochrome c (CytC) (bovine heart, 95%), and fibrinogen (human plasma, fraction I, type I, 65%, 85% clottable) were purchased from Sigma Aldrich.

Stock protein solutions were prepared by dissolving each respective protein at 0.5 mg/ml in PBS and were stored at 4 °C for no longer than one week, with the except of IgG, which was stored at -20 °C at 0.5 mg/ml, as suggested by the manufacturer. Working concentrations of protein were prepared by 10-fold dilutions of the stock solutions to 50 μg/mL in PBS pH 7.4 and stored at 4 °C prior to use.

3.1.2 Nanopattern processing on QCM-D crystals

The PS/PB BCPs were modified by thiol-ene photochemistry to include acid, amine, amide, or captopril moieties. The synthesis of these functionalized polymers is described elsewhere.[118] Briefly, a 63 kDa-block-33 kDa PS/PB BCP was modified using various thiols and BAPO photoinitiator. These polymers are subsequently referred by the R-group grafted onto the PS/PB BCP, ie. PS/PB-Acid in the case of poly(styrene)-block-poly(butadiene-graft-thioglycolic acid). After purification and drying, the polymers were dissolved at 0.5 wt% in suitable solvents or solvent mixtures and spin coated at 2000 rpm onto either silicon wafers or gold coated QCM crystals. PS was dissolved at 0.5 wt% in toluene and PEAA was dissolved at 1 wt% in THF and spin coated at 2000 rpm. Films were dried overnight under house vacuum and baked at 80 °C for 30 minutes to promote film adhesion before protein adsorption experiments.

Tapping mode atomic force microscopy (AFM) was used to image the surface topography of spin coated BCP films using an Asylum MFP-3D system. VistaProbe AFM tips were purchased from Nanoscience Instruments with a nominal tip radius less than 10 nm, spring constant of 48 N/m, and resonant frequency of 190 kHz. 2 x 2 μm scans were completed at 1 Hz with a resolution of 512 x 512 pixels. AFM was performed with the same scanning parameters in PBS after equilibration for 2 hours, using Olympus PSA400 tips with a nominal radius less than 20 nm, 0.08 N/m spring constant, and resonant frequency of 11 kHz.

3.1.3 Static contact angle measurement

Water contact angles were measured with a Ramé Hart goniometer using 18.2 MΩ deionized water. Prior to experimentation, films were acclimated to PBS solutions for 2 hours according to previous procedures for similar systems.[119] After incubation, films were flash dried using compressed nitrogen before placing a ~1 μL deionized water drop onto the film via needle for measurement. At least 10 measurements were made on each polymer surface and water contact angles were quantified using DropImage software. The data represents the mean static contact angle and includes the standard error of the mean.

3.1.4 Quartz crystal microbalance with dissipation

QCM-D measurements were recorded using a QSense Auto E4. An Ismatec multichannel peristaltic pump dispersed buffer and protein solutions at 100 μL/min over AT-cut 4.95 MHz Au-coated quartz crystals obtained from QSense (Sweden).

An automated program was produced with the AutoE4 controller in the QSoft software to obtain a stable baseline in PBS, followed by a one hour adsorption, and completed with a 30 minute PBS wash to obtain a new baseline.

Due to the experimental set-up for static adsorption, real-time monitoring was not feasible without submitting proteins to dynamic conditions. Each run consisted of a 30 minute PBS wash, one hour adsorption, and a final PBS rinse as in the dynamic experiments. Frequency and dissipation were measured before and after adsorption and data files were stitched together in the QTools software. QCM-D data was fit through the QTools software provided from QSense using a one layered Voigt viscoelastic model. A minimum of 4 adsorption curves were recorded for proteins on each respective material. Dissipation versus frequency changes are plotted every 30 points. Deviations from linear behavior were determined using regressions to determine the slope, intercept, and the R^2 value.

Gold QCM-D crystals were reused after each experiment using a cleaning technique recommended by the manufacturer. After a 2% SDS rinse within the sample loop, QCM-D crystals were washed with deionized water, dried with nitrogen, and exposed to ultraviolet light/ozone (UVO) for 20 minutes in a Bioforce Nanosciences Procleaner (Ames, IA). The crystals were cleaned with an NH_4OH/H_2O_2/water (1/1/5 v/v/v) piranha solution at 75 °C for 10 minutes. The crystals were again washed with deionized water, dried with a stream of nitrogen, and baked in UVO for 20 minutes. QCM-D flow cell modules were washed with 2% SDS, deionized water, and dried with nitrogen between experiments before starting a new experimental run.

3.1.5 Statistical Analysis

Water contact angle and protein adsorption values were compared to determine statistical significance using ANOVA combined with Tukey's multiple comparisons test. Statistically significant data are reported using 95% confidence intervals after inputting raw data into Origin software. Within each comparison test, the seven different polymers were compared and their significance as related to the PS, PS/PB and PEAA controls are reported.

3.2 Results and Discussion

3.2.1 Characterization

As described previously, thiol-ene chemistry was used to graft functional groups onto the pendant vinyl group of PS/PB, including an acid, amide, amine, and captopril. Quasi-cylindrical BCP nanopatterns were formed on QCM crystals or silicon wafers using suitable solvents previously established.[118] Figure 3.1 displays dry AFM images of the surfaces, not including the PS films due to insignificant topographical variation. These cylindrical patterns had average center to center distances in the range of 80 nm, with the PS/PB stock BCP having slightly smaller domains. Films consisting of PS and a PEAA random copolymer served as unpatterned controls for determining the mechanism of protein adsorption on nanopatterns.

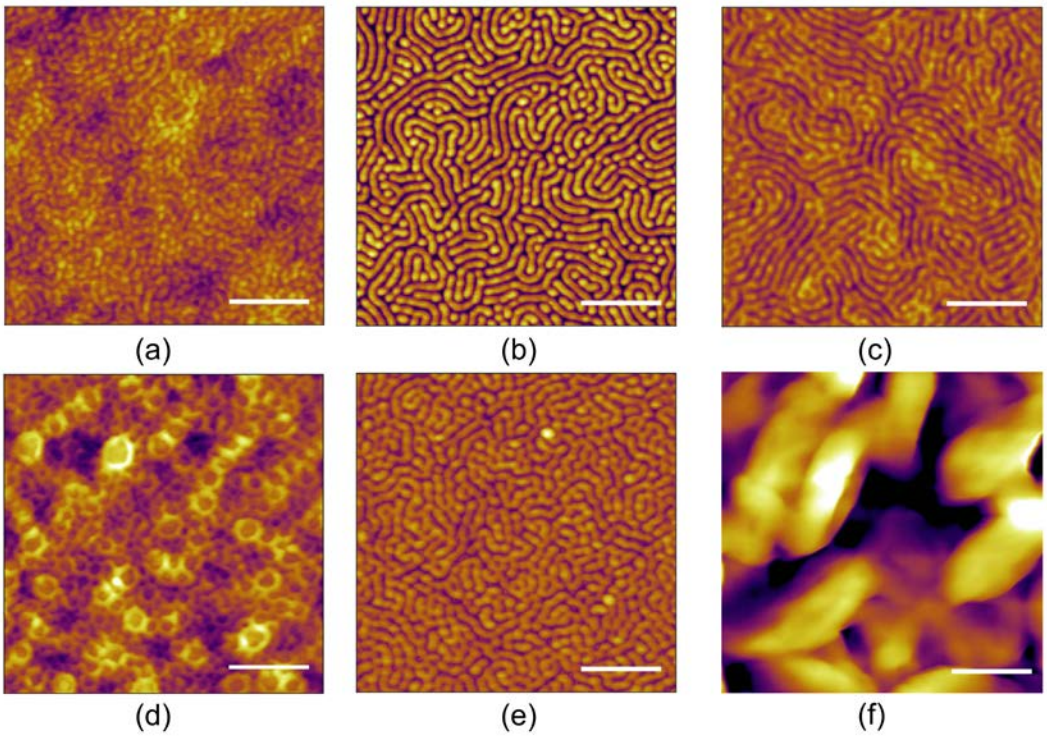

Figure 3.1. Atomic force micrographs of nanopatterned block copolymers and unpatterned controls. (a) PS/PB. (b) PS/PB-Amide. (c) PS/PB-Acid. (d) PS/PB-Amine. (e) PS/PB-Captopril. (f) PEAA. Scale bars: 500 nm.

Initial static measurements from dry films showed little contact angle differences between the thiol grafted BCPs and the control groups (not shown). Xu et. al has shown that buffer equilibration significantly decreased water contact angles for amphiphilic BCP systems after flash drying to vitrify microdomains.[119] Since succeeding experiments conducted in this work were measured at pH 7.4 in PBS after swelling, determination of the contact angles under these conditions was deemed more relevant and conducted in this manner.

Table 3.1 exhibits the water contact angles of the films used in this study. The contact angles of the hydrophobic polymers such as the PS, PEAA, and PS/PB BCP

Polymer	Contact Angle ± SEM
PS/PB-Amide	66.9 ± 1.4
PS/PB-Acid	36.5 ± 1.5
PS/PB-Captopril	30.1 ± 0.8
PS/PB-Amine	56.0 ± 0.9
PS/PB	98.3 ± 0.7
PS	81.3 ± 0.5
PEAA	98.1 ± 2.7

Table 3.1. Static water contact angle measurements of the polymeric surfaces described in this study.

were found to be 81, 98, and 98°, respectively. Despite PBS equilibration of these surfaces, contact angles remained generally unchanged and agreed with literature values.[120-122] Contact angles for the amide, acid, captopril, and amine modified BCPs were 67, 37, 30, and 56°, respectively. The PBS equilibration of the BCPs and controls before contact angle measurement confirmed that only surfaces with polar or charged moieties were sensitive to this handling. Compared to unmodified PS/PB, the thiol grafted BCPs showed large decreases in the contact angle, suggesting increased hydrophilicity. The contact angle of the acid modified polymer resembled values obtained from a poly(styrene)-block-poly(acrylic acid) (PS/PAA) BCP described previously.[119] While not strictly equivalent, plasma polymerized poly(allyl amine) films have also shown similar contact angles to the PS/PB-Amine surface.[123]

Figure 3.2 shows AFM characterization of the patterned and unpatterned films after PBS equilibration. The PS/PB, PS/PB-Amide, and PS films generally maintained their structure after the introduction of buffer. In the case of PS/PB-

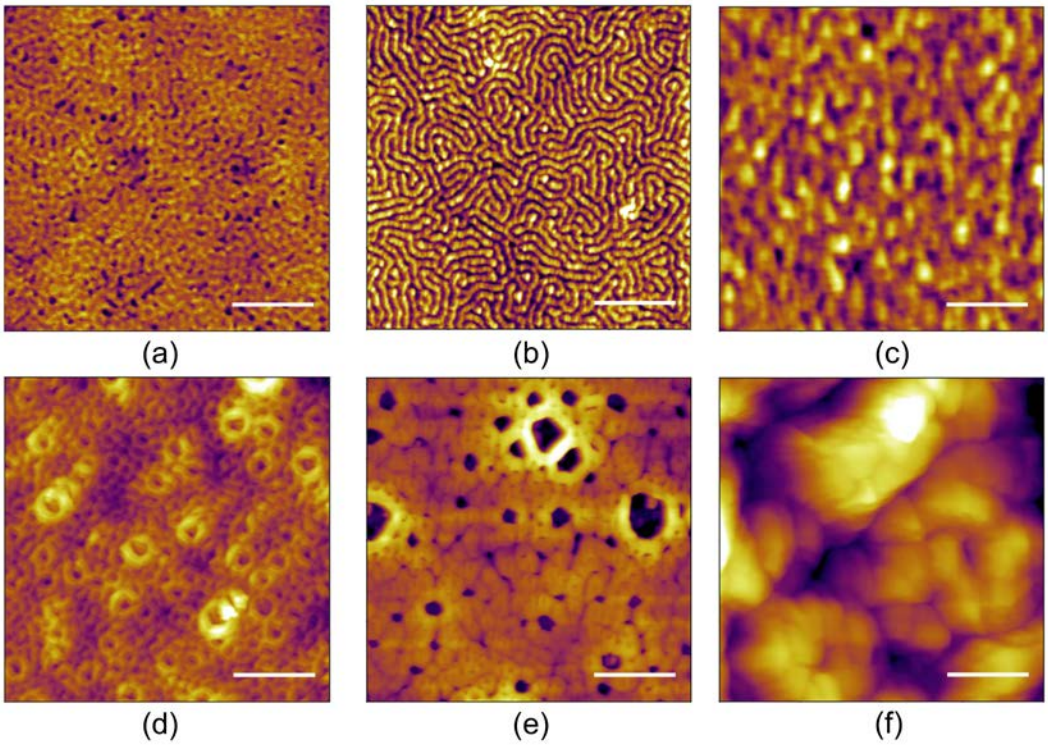

Figure 3.2. Atomic force micrographs of nanopatterned block copolymers and unpatterned controls imaged in PBS buffer . (a) PS/PB. (b) PS/PB-Amide. (c) PS/PB-Acid. (d) PS/PB-Amine. (e) PS/PB-Captopril. (f) PEAA. Scale bars: 500 nm.

Acid, Amine, and Captopril, varying degrees of swelling induced surface structure changes were observed after PBS incubation. The PS/PB-Acid surface swelled enough that little resemblance to the initial dry pattern remained. The contact angles previously mentioned confirmed that wettability was considerably enhanced after acid grafting. The decreased contact angles originate from selective block swelling that suggests the formation of an acid enriched surface layer after buffer equilibration.[108] The possibility of an acid enriched surface layer may validate the disappearance of the microphase-separated morphology on PS/PB-Acid film surfaces after both lateral and vertical swelling.

The PS/PB-Captopril films showed swelling that somewhat distorted the initial quasi-cylindrical pattern and resulted in dimple-like structures. The degree of bidirectional swelling for the PS/PB-Captopril films may be smaller than PS/PB-Acid, which could explain the retention of microphase-separated morphologies in swollen films. The PS/PB-Amine polymer displayed minor swelling from AFM despite a large decrease in the contact angle relative to the PS/PB BCP. Decreased swelling in PS/PB-Amine may originate from the hydrophobic alkyl groups surrounding the tertiary amine.

3.2.2 Static Protein Adsorption

The isoelectric point (pI) and molecular weight of the proteins used in this study are summarized in Table 3.2. Proteins far from their isoelectric points typically exhibit charge-dependent behavior, which applies to BSA, fibrinogen, and CytC.[124] BSA, fibrinogen, and IgG are negatively charged proteins at pH 7.4, while CytC is positively charged. Based on electrostatic interactions, the PS/PB-Acid and Captopril surfaces would be expected to reduce BSA and fibrinogen adsorption, while the

Protein	Source	pI	MW (kDa)
Serum Albumin	Bovine	4.9	66
Fibrinogen	Human	5.5	340
Cytochrome C	Bovine	10.5	12.2
Immunoglobulin G	Human	6.5	150

Table 3.2. Property summary of the proteins investigated in this study. The isoelectric points (pI) and molecular weight (MW) are shown to distinguish between the large size and charge differences.

PS/PB-Amine polymer would strengthen deposition. Conversely, PS/PB-Acid and Captopril would electrostatically attract CytC, while the PS/PB-Amine surface would repel CytC.

The proteins in this work were chosen for a wide variety of charge, MW, and stability against denaturation. Additionally, the presence of albumin, fibrinogen, and IgG in plasma makes their use relevant to the study of blood contacting biomaterials. Albumin can serve as a passivation layer that inhibits coagulation.[125] As discussed in Chapter 1.3.2, fibrinogen adsorption on biomaterials can induce coagulation. Finally, IgG adsorption values can provide information about the immunological response and potential contact activation caused by the BCP surfaces. CytC was used in these studies to include a positively charged protein whose properties have been thoroughly characterized.

Figure 3.3 shows the average protein adsorption densities completed under static conditions. BSA adsorption on the various polymer surfaces was in the range of 1000-2500 ng/cm^2. PS/PB-Amine showed statistically increased BSA adsorption over the PS/PB, PS, and PEAA controls. Otherwise, BSA static adsorptions were fairly consistent between the various polymer surfaces. BSA adlayers on PS/PB-Amine increased relative to uncharged and negatively charged controls, potentially due to electrostatic attraction to the positively charged surface. Additionally, the PS/PB-Amine surface adsorbed statistically higher amounts of BSA compared to the negatively charged PS/PB-Acid and Captopril.

Fibrinogen adlayers were found to vary from approximately 2000-3000 ng/cm^2. Statistically increased fibrinogen adsorption was observed for the PS/PB-Acid

polymer in comparison to PS/PB and PEAA. Fibrinogen adsorption statistically decreased on PS/PB-Captopril and PS/PB compared to PS. However, fibrinogen adsorption increased after contact with PS/PB-Acid, which contradicts the electrostatic repulsion expected between a negatively charged surface and protein.

While there is no statistical variance between some of the negative and positively charged BCPs, electrostatic forces clearly influenced adsorption on the nanopatterned surfaces. Marginal differences were seen for both CytC and IgG adsorption, with ranges between 500-1200 ng/cm^2 and 1200-2400 ng/cm^2, respectively. The adsorption values for both CytC and IgG were similar between most of the surfaces.

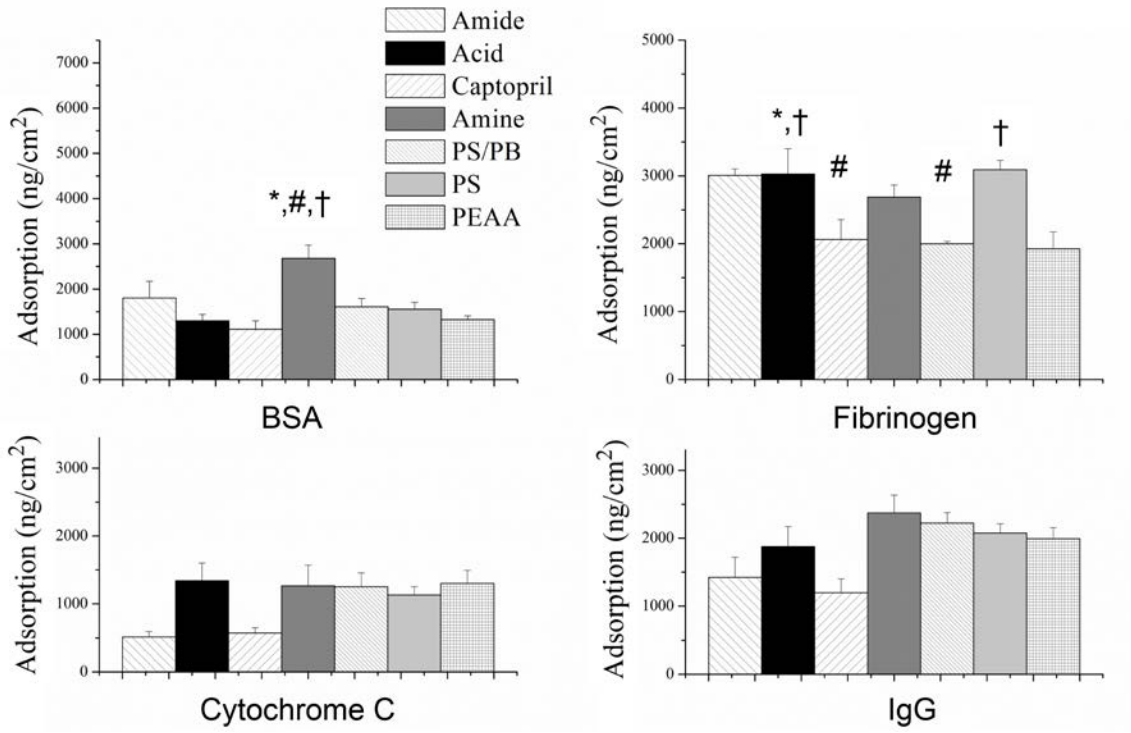

p<0.05 for n=4 (* - PS/PB; # - PS; † - PEAA)

Figure 3.3. Protein densities for the polymeric surfaces completed under static conditions

The exception was statistically higher IgG adsorption on PS/PB-Amine compared to the captopril modified surface.

The theoretical monolayer adsorption limit of BSA is 360 ng/cm^2 for side-on type and 900 ng/cm^2 for end-on adsorption.[126] The theoretical limit of fibrinogen adsorption is approximately 180 ng/cm^2 for side-on type and 1700 ng/cm^2 for end-on type adsorption.[127] The monolayer densities of IgG and CytC are both approximately 300 ng/cm^2.[128, 129] The close-packed densities for BSA and fibrinogen are larger than IgG and CytC due to higher asymmetry in their spatial dimensions.

The results from static adsorption experiments show that large concentrations of protein adsorbed to some of the polymer surfaces. Within experimental errors, BSA typically formed a monolayer on the polymer surfaces, with the exception of PS/PB-Amine. Static adsorption of fibrinogen increased to multiple layers on PS/PB-Acid, Amide, and PS. In the case of CytC, approximate monolayers were formed on all surfaces within experimental error. Finally, multiple layers of IgG were formed on all the surfaces investigated.

Despite swelling of the polyelectrolytes, the extent is not significant enough to increase the close-packed density of a monolayer according to AFM measurements. However, often these polyelectrolyte BCPs adsorbed more protein than one monolayer. Polyelectrolyte chains have been hypothesized to repel one another and increase the porosity of the swollen polymer layer, which would not arise during AFM imaging.[130] The porosity may allow for proteins to penetrate through interstitial spaces and increase adsorption beyond a monolayer. Additionally, large adsorption

values may suggest that proteins are forming multilayered aggregates with one another over an adsorbed monolayer on some surfaces.

3.2.3 Adsorption under flow

In order to describe protein adsorption on material surfaces that encounter blood flow, QCM-D experiments were conducted to investigate protein adlayers under dynamic conditions. Representative raw QCM-D data are shown in Figure 4 for BSA on the polymer surfaces. All overtones were utilized in the viscoelastic models with the exception of the 1st overtone. The frequency decreases upon mass deposition and the dissipation shifts depending on the viscoelastic properties of the adsorbed layer. The hydrophobic polymer surfaces (PS/PB, PS/PB-Amide, PS, PEAA) demonstrated exponential frequency decay that saturated within minutes of protein introduction, shown in Figure 3.4a. The polyelectrolytes (PS/PB-Acid, Captopril, Amine) exhibited an inflection in frequency reduction from an initial exponential decay to a linear decrease until the final PBS rinsing step.

Large dissipative changes were observed for BSA adsorption on the polyelectrolytes, depicted in Figure 3.4b. The hydrophobic and uncharged polymers showed small dissipative changes along the order of 10^{-6}. Dissipative changes on the BCP polyelectrolytes were an order of magnitude higher for BSA adsorption when compared to the hydrophobic surfaces. The exception for the polyelectrolytes was the PS/PB-Amine surface, which showed significantly decreased dissipation during the adsorption process. The data suggests that BSA adlayers on the hydrophobic

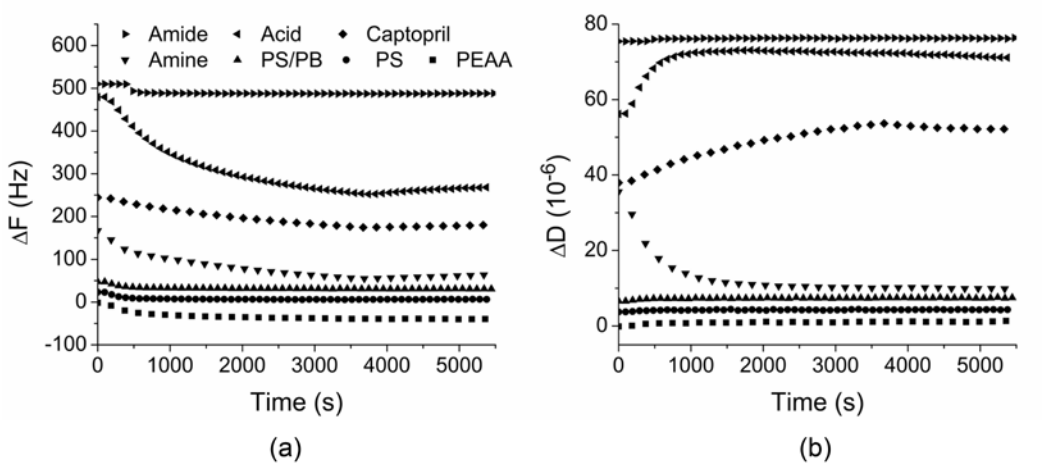

Figure 3.4. Raw QCM-D data from BSA adsorptions (5th overtone). a) Frequency changes show increased mass on the polymer surfaces. b) Dissipative element shows increased viscoelasticity for a majority of the surfaces

polymers were fairly rigid in comparison to the highly viscoelastic BSA adlayers on PS/PB-Acid and Captopril. The physical mechanism and discussion of the adsorption induced dissipation shift will be discussed in the succeeding section.

After collecting raw frequency and dissipation data, these data points were inputted into the Voigt viscoelastic models within the QTools software. Figure 3.5 displays the fitted results for the BCPs, PS, and PEAA for BSA, fibrinogen, CytC, and IgG experiments, respectively. BSA adsorption on PS/PB-Acid, Captopril and Amine BCPs were significantly increased to 1000-3000 ng/cm^2, compared to ~300 ng/cm^2 for both PS and the stock BCP controls. The PS/PB-Amide, Captopril, PS/PB, PS, and PEAA surfaces consisted of a monolayer or less within experimental error. However, the PS/PB-Acid and Amine surfaces adsorbed in excess of a monolayer. Fibrinogen adsorption significantly increased for the acid modified polymer to a

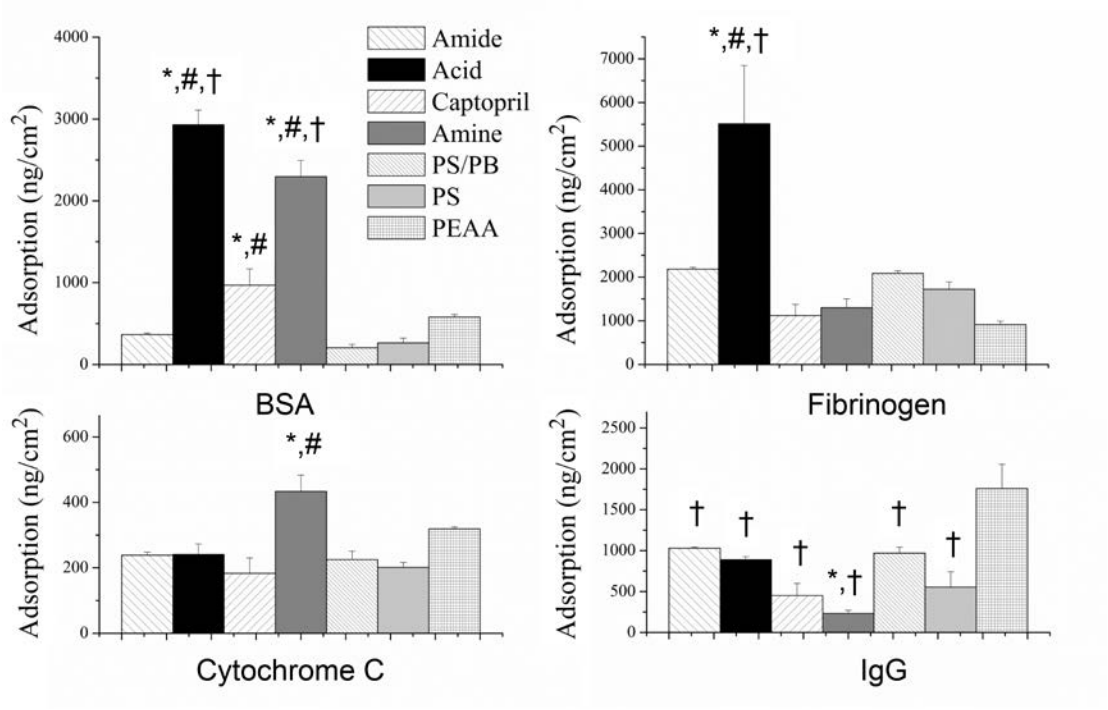

Figure 3.5. Protein adsorption data from QCM-D completed at 100 µL/min on polymer surfaces.

level of 5500 ng/cm^2 compared to densities of 1500-2000 ng/cm^2 for the stock BCP and PS. PS/PB-Amine and Captopril BCPs showed slight decreases in fibrinogen adsorption compared to controls and the amide BCP. The surfaces consisted of fibrinogen monolayers with the exception of PS/PB-Acid, whose density was significantly higher.

CytC adsorption remained fairly constant and was in the range of 175-300 ng/cm^2. The exception was the aminated polymer, which showed a significant increase to ~430 ng/cm^2. Considering the experimental error, these densities fall within the range of CytC monolayers for all surfaces.

IgG adsorption on the polymer surfaces were in the range of 230-1750 ng/cm^2. The aminated polymer exhibited the lowest density, which significantly varied from the PS/PB control. The PS/PB-Captopril, Amine, and PS control surfaces adsorbed IgG within a monolayer, while PS/PB-Amide, Acid, PS/PB, and PEAA all consisted of adlayers in excess of a monolayer.

Now that the adsorption densities for each respective surface and protein pair were introduced, these data will be discussed along with potential implications of the results. Thus far frequency and dissipation data were exclusively used to describe relative gravimetric differences between polymer surfaces for a given protein. However, these parameters can also provide qualitative information about adlayer structure. The succeeding section will describe some of the possible mechanisms occurring during the adsorption process.

3.2.4 Dissipation versus Frequency plots

Dissipation versus frequency plots (D-f plots) detail time independent processes and have been used to determine whether multiple kinetic regions occur during adsorption.[55] The slope of D-f plots describes the relative rigidity or viscoelasticity of adlayers. Large $\Delta D/\Delta f$ values suggest that the adsorbed layer is highly dissipative or viscoelastic, as described in Chapter 1.3.2.2. Likewise, small $\Delta D/\Delta f$ are indicative of rigid adlayers. Due to the non-specificity of QCM-D, these measurements could exclusively refer to the protein layer or contain some contribution from the polymer coatings.

Figure 3.6 depicts the D-f plots for the surfaces during BSA adsorptions. The hydrophobic polymers such as PS/PB, PS/PB-Amide, PS, and PEAA displayed linear relationships between dissipation and frequency. Regressions for these relations exhibited R^2>0.95. Additionally the slope, or ΔD/Δf, for these three surfaces was similar, suggesting that the adlayers have similar properties. The PS/PB-Acid surface exhibited an exponential increase in dissipation during BSA adsorption. Conversely, PS/PB-Amine exhibited an exponential decrease in dissipation.

Linear D-f plots are typical for BSA adsorptions on hydrophobic polymers. After

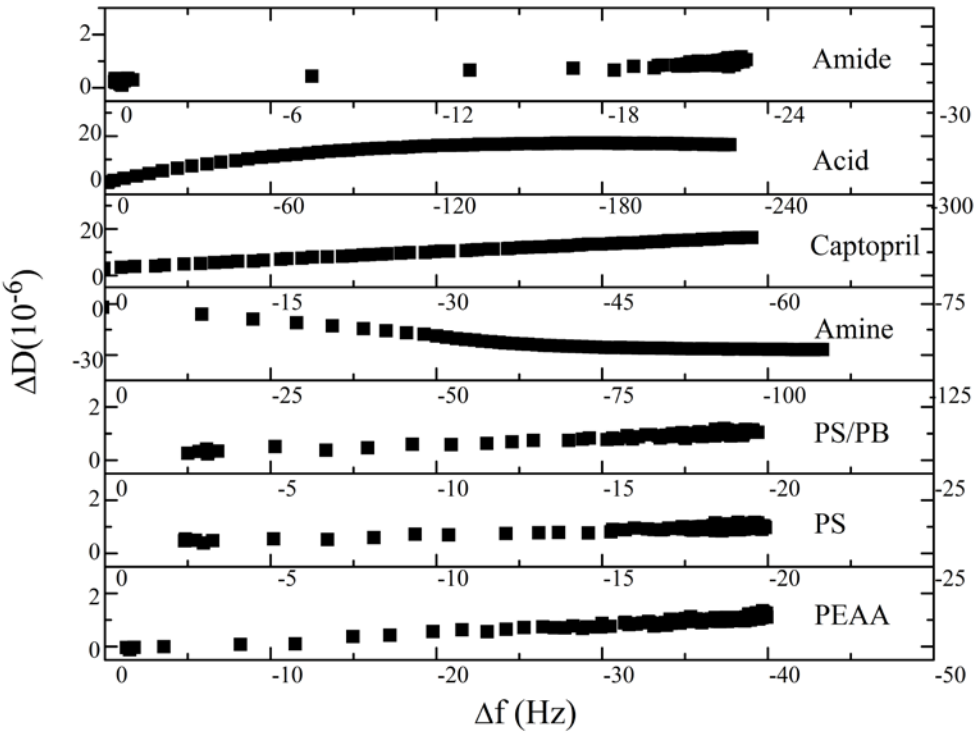

Figure 3.6. Dissipation versus frequency plots of bovine serum albumin adsorption on the BCP patterns and controls.

the frequency saturated, marginal dissipation increases occurred which may be due to small conformational changes or denaturation of the adlayer. The partial denaturation of hydrophobic proteins such as BSA on hydrophobic surfaces has been confirmed by complimentary techniques, where protein subdomains become exposed.[124] As discussed in Chapter 1.3.2, BSA dehydration and partial denaturation may occur from bonding of complimentary hydrophobic domains on each respective structure.[19]

For the cases of the acid and amine modified PS/PB BCPs, the landscape becomes more complex due to the charged nature of the nanostructured surfaces. As the frequency of PS/PB-Acid decreased, an exponential increase in dissipation occurred. This suggests that the adlayer became more viscoelastic with time and may be caused by denaturation of BSA as adsorption occurs. While these are hypotheses, QCM-D cannot definitively discern whether either scenario is accurate.

The PS/PB-Amine polymer exhibited an exponential decrease in dissipation as frequency decreased for BSA adsorption. Decreased dissipation during protein adsorption may suggest either dehydration of the adlayer, collapse of the swollen polymer, or some combination of the two. With a water contact angle of 56°, the PS/PB-Amine surface still maintains some hydrophobic character along with its positive charge. BSA is both sensitive to denaturation on hydrophobic surfaces and may be electrostatically attracted to the cationic surface. This attraction may induce collapse of the polymer-protein but requires a complimentary technique to confirm this. The D-f plots for fibrinogen are shown in Figure 3.7. Similar to BSA, linear relationships between dissipation and frequency were observed for fibrinogen adlayers on hydrophobic PS/PB, PS/PB-Amide, PS, and PEAA surfaces. An

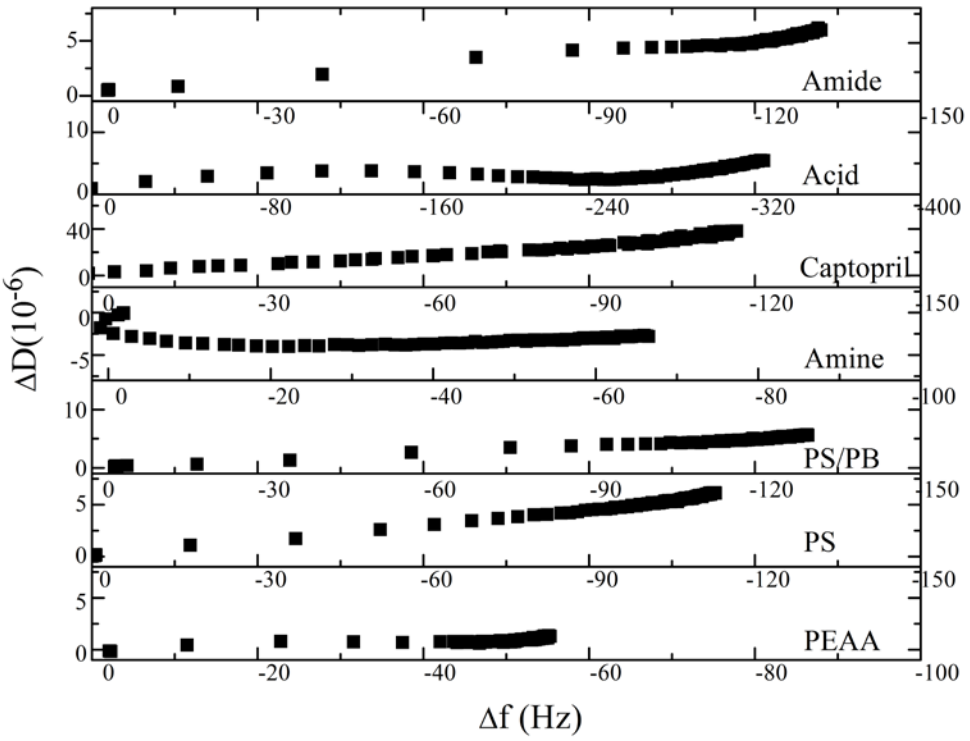

Figure 3.7. Dissipation versus frequency plots of adsorbed fibrinogen on the BCP patterns and controls.

inflection in the dissipation was present for these surfaces when frequency leveled, which is suggestive of partial denaturation.[55] The stability of fibrinogen against denaturation is lower compared to BSA due to structural heterogeneity in the tripeptide. The preferential affinity of one chain for a surface has been suggested as the cause of lower fibrinogen stability during adsorption processes.[131]

Deviations from typical adsorption isotherms were also observed for the PS/PB-Acid and PS/PB-Amine surfaces after fibrinogen adsorption. The PS/PB-Acid exhibited a sinusoidal like dissipation versus frequency relationship. The first phase of this adsorption mimics that of hydrophobic controls and may be approximated as a monolayer. Subsequently, either fibrinogen or PS/PB-Acid partially dehydrates before continuing to adsorb more protein with increased dissipation. PS/PB-Amine exhibited very similar behavior for fibrinogen as was discussed for BSA adsorption.

The D-f plots for CytC demonstrated behavior more typical of rigid protein adlayers, as shown in Figure 3.8. The hydrophobic polymers had nearly linear

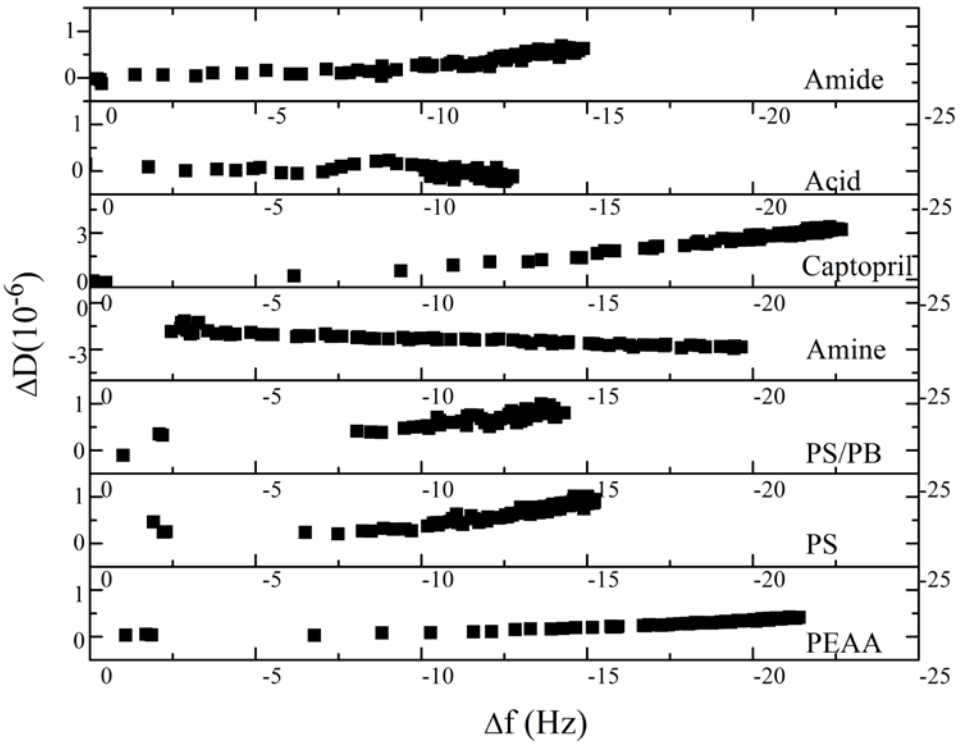

Figure 3.8. Dissipation versus frequency plots of adsorbed cytochrome c on the BCP patterns and controls.

profiles that leveled around a monolayer. The PS/PB-Acid and Amine polymers both exhibited approximate monolayers, however both of their dissipations decreased during the adsorption process. For the negatively charged PS/PB-Acid, perhaps the opposite charge of CytC induces collapse of the protein-polymer complex, but this would require further experiments for confirmation.

The dissipative versus frequency relationships for IgG were all generally linear, as shown in Figure 3.9, with the exception of PS/PB-Amine. PS/PB-Amine exhibited the dissipation loss observed with every protein with this surface. Despite the linear

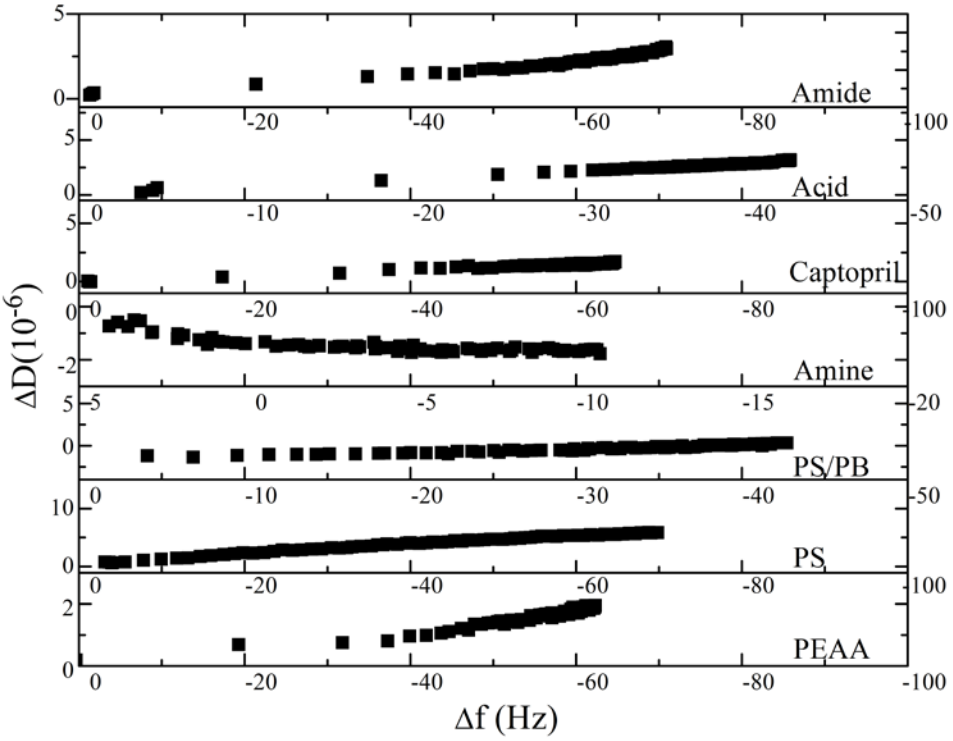

Figure 3.9. Dissipation versus frequency plots of adsorbed immunoglobulin g on the BCP patterns and controls.

relationships, densities greater than a monolayer adsorbed onto most of the surfaces under investigation. Since no inflection was present in the D-f plots, little can be inferred from these relationships in terms of qualitative discussions of its conformation. The mechanism of multilayered IgG adsorption is still under investigation.

3.2.5 Implications of Protein Adsorption on BCPs

The presence of charged groups significantly increased BSA and fibrinogen adsorption over uncharged polymers. BSA and fibrinogen values were especially high on the PS/PB-Acid polymer despite both the surface and proteins containing negative charges. Soft proteins such as BSA and fibrinogen can bind to polymer surfaces regardless of charge implications due to their low stability, even resisting electrostatic repulsion.[19, 132] This behavior was hypothesized to result from protein secondary structure changes after irreversible binding that exposes motifs not typically present on the protein's surface.[133] Another theory about large depositions on like-charged polymer protein complexes focus on the charge anisotropy inherent in proteins.[134] Computational models from other studies indicated that uniformly charged surfaces could not predict the behavior of like-charged proteins and polymers and that charge on proteins most likely exists in patches.[17]

From these data, some conclusions can be drawn about the role of electrostatic charge when confined within a BCP nanopattern. While electrostatic interactions did not necessarily guide protein adsorption, they certainly affected the formation of

protein layers. Under static conditions, protein adsorption often occurred in excess of monolayers without regard for electrostatics. Electrostatic interactions seemed to play a more significant role under dynamic conditions, where the polyelectrolyte BCPs adsorbed excess amounts of BSA and fibrinogen.

The consequences of both albumin and fibrinogen adsorption on biomedical polymer surfaces are imperative to understand since they are the most abundant plasma proteins in circulation. Albumin coated surfaces are long known to act as thrombo-resistant passivation layers, which may be beneficial for biomedical coatings.[125] Conversely, fibrinogen was previously discussed in Chapter 1.3.2 to be an essential component of the coagulation cascade. In fact, the denaturation of adsorbed fibrinogen may enhance the coagulation response, which could present safety hazards in the context of medical devices.

3.3 Conclusion

A model system for determining the effects of nanopatterned chemistries on protein adsorption was developed through modular thiol-ene chemistry. AFM characterization and water contact angle measurement showed the ability to control surface patterns while varying charge and hydrophobicity. The introduction of charge caused selective swelling of charged blocks and decreased water contact angles. QCM-D experiments suggested that some polyelectrolyte BCPs disproportionately increased protein adsorption of proteins with low stability when compared to uncharged and/or unpatterned controls. The mechanism of increased adsorption is believed to result from protein multilayer deposition due to either dehydration or collapse of both polymer and protein. Qualitative frequency and dissipation analysis

suggested that charged nanopatterns may have larger denaturing effects on proteins with low solution stability, such as BSA and fibrinogen, compared to more rigid proteins such as CytC.

4 : Contributions and Future Work

4.1 Contributions

This dissertation details the synthesis, characterization, and applications of a modular system of nanopatterned BCPs. Photochemical thiol-ene chemistry was used to modify poly(styrene)-block-poly(1,2-butadiene) (PS/PB) BCPs to develop a model system of nanopatterns where the chemistry could be tuned in a modular fashion. PS/PB was modified with a model monomer, boc-cysteamine, to determine the effect of PB molecular weight on the functionalization degree and PDI. This dissertation showed that as the MW of the PB block increased, the propensity for gelation also increased. After determination that high thiol excess was required, polymers with acid, amine, and captopril functionalizations were successfully synthesized. Modular BCP nanopatterns could be processed from solvents found suitable using an iterative approach.

The second portion of this dissertation sought to demonstrate whether protein adsorption was affected by modular chemical nanopatterns. Liquid AFM imaging and contact angle measurements confirmed the large degree of swelling by the grafted BCPs despite their hydrophobic backbones. Experiments with a quartz crystal microbalance with dissipative monitoring showed that BCP nanopatterns often adsorbed disproportionate amounts of protein after modification with polyelectrolytes, often in excess of monolayers. Experiments done under static and flow conditions confirmed the nuances of testing protocol. This may suggest that medical device submissions undergo *in vitro* testing under simulated conditions.

While the synthesis was limited to a few representative groups, several other functional groups could be combined with this technique to further examine the interface between synthetic polymers and biomacromolecules. Previous thiol-ene reactions on PB polymers either took approximately 24 hours for thermal initiation or UV initiated reactions were limited to low molecular weight polymers. The photochemical thiol-ene reaction presented in this dissertation is complete within one hour and is capable of modifying high molecular weight polymers. The wide scope of the synthetic scheme permits the creation of several nanopatterns from one source material. Despite much work remaining to characterize the interface between synthetic polymers and proteins, this work is one of the first to use a label-free technique to observe the relationship between systematically varied modular nanopatterns surfaces and proteins.

4.2 Future Work

While long periods of time were required to develop this system, certainly there are numerous studies that could be completed after its characterization was described in this dissertation. Among them include the systematic variation of the functionalization degree, which was an elusive prospect in this research. Suggestions for controlling the grafting yield include the use of docile R-groups, such as thiolated alkanes, which could act as spacers for functional groups. With their use, successful conversion of double bonds could occur without inducing gelation.

Additional suggested studies could involve the use of antibodies within the QCM-D adsorption setup to quantitatively determine the amount of proteins available for

binding. In terms of primary protein solutions, this could provide some information about what percentage of protein maintains its biological activity. Competitive binding could be assessed using antibodies to determine the relative amount of a specific protein from a complex biofluid such as blood plasma or serum.

After full characterization of the protein response to the BCP nanopatterns, *in vitro* cell culture would provide insightful data on the methods included in the biocompatibility ISO standard. Suggested future experiments should include a comparison of the viability of cells included in ISO-10993 to primary cell cultures like human umbilical vein endothelial cells, which may more accurately depict the cardiovascular environment. Portions of this work were proposed, but remain unfinished.

Another suggestion for future work includes using more recent processing techniques, such as electrospinning. A shortcoming of block copolymer systems is their inability to reach beyond scales of 10-100 nm in terms of domain spacing to systematically vary the length scale of patterns beyond one order of magnitude. Electrospinning could permit the processing of BCP patterns that reach the several hundred nanometer scale with patterns also on the 10-100 nm scale.

5 References

1. Wagner, V.; Dullaart, A.; Bock, A. K.; Zweck, A. *Nat Biotechnol* **2006,** 24, (10), 1211-7.

2. Nel, A. E.; Madler, L.; Velegol, D.; Xia, T.; Hoek, E. M. V.; Somasundaran, P.; Klaessig, F.; Castranova, V.; Thompson, M. *Nature Materials* **2009,** 8, (7), 543-557.

3. Landsiedel, R.; Ma-Hock, L.; Kroll, A.; Hahn, D.; Schnekenburger, J.; Wiench, K.; Wohlleben, W. *Advanced Materials* **2010,** 22, (24), 2601-2627.

4. Buch, E.; Boyle, N. G.; Belott, P. H. *Circulation* **2011,** 123, (11), E378-E380.

5. Bryers, J. D. *Biotechnology and Bioengineering* **2008,** 100, (1), 1-18.

6. ISO-10993, Biological evaluation of medical devices. In 2010.

7. Ratner, B. D., *Biomaterials science : an introduction to materials in medicine*. 2nd ed.; Elsevier Academic Press: Amsterdam ; Boston, 2004; p xii, 851 p.

8. Ratner, B. D. *Biomaterials* **2007,** 28, (34), 5144-7.

9. Vogler, E. A. *Biomaterials* **2011,** 33, (5), 1201-37.

10. Dalsin, J., Messersmith, P. *Materials Today* **2005,** 8, (9), 38-46.

11. Bixler, G. D.; Bhushan, B. *Philosophical Transactions of the Royal Society a-Mathematical Physical and Engineering Sciences* **2012,** 370, (1967), 2381-2417.

12. Wu, Y.; Zhang, M.; Hauch, K. D.; Horbett, T. A. *J Biomed Mater Res A* **2008,** 85, (3), 829-39.

13. Luscher, T. F.; Steffel, J.; Eberli, F. R.; Joner, M.; Nakazawa, G.; Tanner, F. C.; Virmani, R. *Circulation* **2007,** 115, (8), 1051-1058.

14. Greenberg, C. S.; Miraglia, C. C.; Rickles, F. R.; Shuman, M. A. *Journal of Clinical Investigation* **1985,** 75, (5), 1463-1470.

15. Lodish, H. F., *Molecular cell biology*. 6th ed.; W.H. Freeman: New York, 2008; p 1 v. (various pagings).

16. Righetti, P. G.; Caravaggio, T. *Journal of Chromatography* **1976,** 127, (1), 1-28.

17. Asthagiri, D.; Lenhoff, A. M. *Langmuir* **1997,** 13, (25), 6761-6768.

18. Andrade, J. D.; Hlady, V. *Advances in Polymer Science* **1986,** 79, 1-63.

19. Norde, W. *Advances in Colloid and Interface Science* **1986,** 25, (4), 267-340.

20. Donovan, J. W.; Mihalyi, E. *Proc Natl Acad Sci U S A* **1974,** 71, (10), 4125-8.

21. Mrksich, M.; Sigal, G. B.; Whitesides, G. M. *Langmuir* **1995,** 11, (11), 4383-4385.

22. Wagner, M. S.; Horbett, T. A.; Castner, D. G. *Langmuir* **2003,** 19, (5), 1708-1715.

23. Arima, Y.; Iwata, H. *Biomaterials* **2007,** 28, (20), 3074-82.

24. Sigal, G. B.; Mrksich, M.; Whitesides, G. M. *Journal of the American Chemical Society* **1998,** 120, (14), 3464-3473.

25. Balcells, M.; Klee, D.; Fabry, M.; Hocker, H. *Journal of Colloid and Interface Science* **1999,** 220, (2), 198-204.

26. Grinnell, F.; Feld, M. K. *Journal of Biological Chemistry* **1982,** 257, (9), 4888-4893.

27. Wegner, G. J.; Wark, A. W.; Lee, H. J.; Codner, E.; Saeki, T.; Fang, S. P.; Corn, R. M. *Analytical Chemistry* **2004,** 76, (19), 5677-5684.

28. Michael, K. E.; Vernekar, V. N.; Keselowsky, B. G.; Meredith, J. C.; Latour, R. A.; Garcia, A. J. *Langmuir* **2003,** 19, (19), 8033-8040.

29. Steiner, G.; Tunc, S.; Maitz, M.; Salzer, R. *Analytical Chemistry* **2007,** 79, (4), 1311-1316.

30. Paynter, R. W.; Ratner, B. D.; Horbett, T. A.; Thomas, H. R. *Journal of Colloid and Interface Science* **1984,** 101, (1), 233-245.

31. Kondo, A.; Murakami, F.; Higashitani, K. *Biotechnology and Bioengineering* **1992,** 40, (8), 889-894.

32. Homola, J.; Yee, S. S.; Gauglitz, G. *Sensors and Actuators B-Chemical* **1999,** 54, (1-2), 3-15.

33. Wilson, C. J. *Journal of Physics D-Applied Physics* **1974,** 7, (18), 2449-&.

34. Hook, F. *Thesis* **1997**.

35. Sauerbrey, G. *Zeitschrift Fur Physik* **1959,** 155, (2), 206-222.

36. Leskela, M.; Ritala, M. *Thin Solid Films* **2002,** 409, (1), 138-146.

37. Martin, S. J.; Frye, G. C.; Ricco, A. J.; Senturia, S. D. *Analytical Chemistry* **1993,** 65, (20), 2910-2922.

38. Rodahl, M.; Hook, F.; Kasemo, B. *Analytical Chemistry* **1996,** 68, (13), 2219-2227.

39. Rodahl, M.; Hook, F.; Krozer, A.; Brzezinski, P.; Kasemo, B. *Review of Scientific Instruments* **1995,** 66, (7), 3924-3930.

40. Voinova, M. V.; Rodahl, M.; Jonson, M.; Kasemo, B. *Physica Scripta* **1999,** 59, (5), 391-396.

41. Voinova, M. V.; Jonson, M.; Kasemo, B. *Biosensors & Bioelectronics* **2002,** 17, (10), 835-841.

42. Schmidt, D. J.; Min, Y.; Hammond, P. T. *Soft Matter* **2011,** 7, (14), 6637-6647.

43. Lee, H. S.; Eckmann, D. M.; Lee, D.; Hickok, N. J.; Composto, R. J. *Langmuir* **2011,** 27, (20), 12458-12465.

44. QSense.

45. Ku, D. N. *Annual Review of Fluid Mechanics* **1997,** 29, 399-434.

46. Tsuji, S.; Sugimoto, M.; Miyata, S.; Kuwahara, M.; Kinoshita, S.; Yoshioka, A. *Blood* **1999,** 94, (3), 968-975.

47. Dolatshahi-Pirouz, A.; Jensen, T.; Foss, M.; Chevallier, J.; Besenbacher, F. *Langmuir* **2009,** 25, (5), 2971-2978.

48. George, P. A.; Donose, B. C.; Cooper-White, J. J. *Biomaterials* **2009,** 30, (13), 2449-2456.

49. Hemmersam, A. G.; Rechendorff, K.; Besenbacher, F.; Kasemo, B.; Sutherland, D. S. *Journal of Physical Chemistry C* **2008,** 112, (11), 4180-4186.

50. Lau, K. H. A.; Bang, J.; Kim, D. H.; Knoll, W. *Advanced Functional Materials* **2008,** 18, (20), 3148-3157.

51. Iwamoto, G. K.; Winterton, L. C.; Stoker, R. S.; Vanwagenen, R. A.; Andrade, J. D.; Mosher, D. F. *Journal of Colloid and Interface Science* **1985,** 106, (2), 459-464.

52. Salim, M.; O'Sullivan, B.; McArthur, S. L.; Wright, P. C. *Lab Chip* **2007,** 7, (1), 64-70.

53. Koc, Y.; de Mello, A. J.; McHale, G.; Newton, M. I.; Roach, P.; Shirtcliffe, N. J. *Lab Chip* **2008,** 8, (4), 582-6.

54. Ayela, C.; Roquet, F.; Valera, L.; Granier, C.; Nicu, L.; Pugniere, M. *Biosensors & Bioelectronics* **2007,** 22, (12), 3113-3119.

55. Hook, F.; Rodahl, M.; Kasemo, B.; Brzezinski, P. *Proceedings of the National Academy of Sciences of the United States of America* **1998,** 95, (21), 12271-12276.

56. Voros, J. *Biophysical Journal* **2004,** 87, (1), 553-561.

57. Xia, Y. N.; Whitesides, G. M. *Angewandte Chemie-International Edition* **1998,** 37, (5), 551-575.

58. Merkel, T. J.; Herlihy, K. P.; Nunes, J.; Orgel, R. M.; Rolland, J. P.; DeSimone, J. M. *Langmuir* **2010,** 26, (16), 13086-13096.

59. Zhang, S. *Nature biotechnology* **2003,** 21, (10), 1171-8.

60. Romano, F.; Sciortino, F. *Nat Mater* 10, (3), 171-3.

61. Venkataraman, S.; Hedrick, J. L.; Ong, Z. Y.; Yang, C.; Ee, P. L.; Hammond, P. T.; Yang, Y. Y. *Advanced drug delivery reviews* 63, (14-15), 1228-46.

62. Whitesides, G. M.; Grzybowski, B. *Science* **2002,** 295, (5564), 2418-21.

63. Bates, F. S. *Science* **1991,** 251, (4996), 898-905.

64. Leibler, L. *Macromolecules* **1980,** 13, (6), 1602-1617.

65. Bates, F. S.; Fredrickson, G. H. *Annual Review of Physical Chemistry* **1990,** 41, 525-557.

66. Khandpur, A. K.; Forster, S.; Bates, F. S.; Hamley, I. W.; Ryan, A. J.; Bras, W.; Almdal, K.; Mortensen, K. *Macromolecules* **1995,** 28, (26), 8796-8806.

67. Zheng, W.; Wang, Z. G. *Macromolecules* **1995,** 28, (21), 7215-7223.

68. Forster, S.; Zisenis, M.; Wenz, E.; Antonietti, M. *Journal of Chemical Physics* **1996,** 104, (24), 9956-9970.

69. Painter, P. C.; Coleman, M. M., *Fundamentals of polymer science : an introductory text*. 2nd ed.; Technomic Pub. Co.: Lancaster, Pa., 1997; p xv, 478 p.

70. Hsieh, H. L.; Quirk, R. P., *Anionic polymerization : principles and practical applications*. Marcel Dekker: New York, 1996; p viii, 727 p.

71. Hautekeer, J. P.; Varshney, S. K.; Fayt, R.; Jacobs, C.; Jerome, R.; Teyssie, P. *Macromolecules* **1990,** 23, (17), 3893-3898.

72. Li, M. Q.; Ober, C. K. *Materials Today* **2006,** 9, (9), 30-39.

73. Fasolka, M. J.; Banerjee, P.; Mayes, A. M.; Pickett, G.; Balazs, A. C. *Macromolecules* **2000,** 33, (15), 5702-5712.

74. Knoll, A.; Horvat, A.; Lyakhova, K. S.; Krausch, G.; Sevink, G. J. A.; Zvelindovsky, A. V.; Magerle, R. *Physical Review Letters* **2002,** 89, (3).

75. Lotti, L.; Coiai, S.; Ciardelli, F.; Galimberti, M.; Passaglia, E. *Macromolecular Chemistry and Physics* **2009,** 210, (18), 1471-1483.

76. Justynska, J.; Hordyjewicz, Z.; Schlaad, H. *Macromolecular Symposia* **2006,** 240, 41-46.

77. Frechet, J. M. J. *Science* **1994,** 263, (5154), 1710-1715.

78. Zhang, X.; Xia, J. H.; Matyjaszewski, K. *Macromolecules* **2000,** 33, (7), 2340-2345.

79. Meijs, G. F.; Morton, T. C.; Rizzardo, E.; Thang, S. H. *Macromolecules* **1991,** 24, (12), 3689-3695.

80. Zeng, F. W.; Zimmerman, S. C. *Journal of the American Chemical Society* **1996,** 118, (22), 5326-5327.

81. Killops, K. L.; Campos, L. M.; Hawker, C. J. *Journal of the American Chemical Society* **2008,** 130, (15), 5062-+.

82. Barner-Kowollik, C.; Du Prez, F. E.; Espeel, P.; Hawker, C. J.; Junkers, T.; Schlaad, H.; Van Camp, W. *Angewandte Chemie-International Edition* **2011,** 50, (1), 60-62.

83. Loudon, G. M., *Organic chemistry*. 4th ed.; Oxford University Press: New York, 2002; p 1 v. (various pagings).

84. Goodyear, C. Improvement in the Manufacture of Caoutchouc. 3633, June 15, 1844.

85. Thannhauser, T. W.; Konishi, Y.; Scheraga, H. A. *Analytical Biochemistry* **1984,** 138, (1), 181-188.

86. Kade, M. J.; Burke, D. J.; Hawker, C. J. *Journal of Polymer Science Part a-Polymer Chemistry* **2010,** 48, (4), 743-750.

87. Campos, L. M.; Killops, K. L.; Sakai, R.; Paulusse, J. M. J.; Damiron, D.; Drockenmuller, E.; Messmore, B. W.; Hawker, C. J. *Macromolecules* **2008,** 41, (19), 7063-7070.

88. Cramer, N. B.; Bowman, C. N. *Journal of Polymer Science Part a-Polymer Chemistry* **2001,** 39, (19), 3311-3319.

89. Koo, S. P. S.; Stamenovic, M. M.; Prasath, R. A.; Inglis, A. J.; Du Prez, F. E.; Barner-Kowollik, C.; Van Camp, W.; Junkers, T. *Journal of Polymer Science Part a-Polymer Chemistry* **2010,** 48, (8), 1699-1713.

90. Yang, H.; Jia, L.; Zhu, C. H.; Di-Cicco, A.; Levy, D.; Albouy, P. A.; Li, M. H.; Keller, P. *Macromolecules* **2010,** 43, (24), 10442-10451.

91. Bertin, A.; Schlaad, H. *Chemistry of Materials* **2009,** 21, (24), 5698-5700.

92. Korthals, B.; Morant-Minana, M. C.; Schmid, M.; Mecking, S. *Macromolecules* **2010,** 43, (19), 8071-8078.

93. Wickard, T. D.; Nelsen, E.; Madaan, N.; ten Brummelhuis, N.; Diehl, C.; Schlaad, H.; Davis, R. C.; Linford, M. R. *Langmuir* **2010,** 26, (3), 1923-1928.

94. Uygun, M.; Tasdelen, M. A.; Yagci, Y. *Macromolecular Chemistry and Physics* **2010,** 211, (1), 103-110.

95. ten Brummelhuis, N.; Diehl, C.; Schlaad, H. *Macromolecules* **2008,** 41, (24), 9946-9947.

96. Justynska, J.; Hordyjewicz, Z.; Schlaad, H. *Polymer* **2005,** 46, (26), 12057-12064.

97. Decker, C.; Viet, T. N. T. *Polymer* **2000,** 41, (11), 3905-3912.

98. Justynska, J.; Schlaad, H. *Macromolecular Rapid Communications* **2004,** 25, (16), 1478-1481.

99. Passaglia, E.; Donati, F. *Polymer* **2007,** 48, (1), 35-42.

100. David, R. L. A.; Kornfield, J. A. *Macromolecules* **2008,** 41, (4), 1151-1161.

101. Shortt, D. W. *Journal of Liquid Chromatography* **1993,** 16, (16), 3371-3391.

102. Young, R. J.; Lovell, P. A., *Introduction to polymers*. 2nd ed.; Chapman & Hall: London ; New York, 1991; p x, 443 p.

103. Flory, P. J., *Principles of polymer chemistry*. Cornell University Press: Ithaca,, 1953; p 672 p.

104. Gaur, U.; Wunderlich, B. *Macromolecules* **1980,** 13, (2), 445-446.

105. Yeh, Y. S.; James, W. J.; Yasuda, H. *Journal of Polymer Science Part B-Polymer Physics* **1990,** 28, (4), 545-568.

106. Puskas, J. E.; Antony, P.; Kwon, Y.; Kovar, M.; Norton, P. R. *Macromolecular Symposia* **2002,** 183, 191-197.

107. Israelachvili, J. N., *Intermolecular and surface forces*. 3rd ed.; Academic Press: Burlington, MA, p xxx, 674 p.

108. Park, J. H.; Sun, Y. J.; Goldman, Y. E.; Composto, R. J. *Macromolecules* **2009,** 42, (4), 1017-1023.

109. Rugar, D.; Hansma, P. *Physics Today* **1990,** 43, (10), 23-30.

110. Gross, L.; Mohn, F.; Moll, N.; Liljeroth, P.; Meyer, G. *Science* **2009,** 325, (5944), 1110-1114.

111. Demirel, A. L.; Schlaad, H. *Polymer* **2008,** 49, (16), 3470-3476.

112. Fisher, J. P.; Tirnmer, M. D.; Holland, T. A.; Dean, D.; Engel, P. S.; Mikos, A. G. *Biomacromolecules* **2003,** 4, (5), 1327-1334.

113. Fisher, J. P.; Holland, T. A.; Dean, D.; Mikos, A. G. *Biomacromolecules* **2003,** 4, (5), 1335-1342.

114. Tedder, J. M. *Angew. Chem.-Int. Edit. Engl.* **1982,** 21, (6), 401-410.

115. Dimarzio, E. A.; Guttman, C. M. *Macromolecules* **1987,** 20, (6), 1403-1407.

116. Kim, S. H.; Misner, M. J.; Xu, T.; Kimura, M.; Russell, T. P. *Advanced Materials* **2004,** 16, (3), 226-+.

117. Zhang, X.; Metting, C. J.; Briber, R. M.; Weilnboeck, F.; Shin, S. H.; Jones, B. G.; Oehrlein, G. S. *Macromolecular Chemistry and Physics* **2011,** 212, (16), 1735-1741.

118. Silverstein, J. S., Casey, B.J., Natoli, M.E., Dair, B.J., Kofinas, P. *Macromolecules* **2012,** 45, (7), 3161-3167.

119. Xu, C.; Wayland, B. B.; Fryd, M.; Winey, K. I.; Composto, R. J. *Macromolecules* **2006,** 39, (18), 6063-6070.

120. Ellison, A. H.; Zisman, W. A. *Journal of Physical Chemistry* **1954,** 58, (6), 503-506.

121. Janorkar, A. V.; Luo, N.; Hirt, D. E. *Langmuir* **2004,** 20, (17), 7151-7158.

122. Luzinov, I.; Julthongpiput, D.; Tsukruk, V. V. *Macromolecules* **2000,** 33, (20), 7629-7638.

123. Aizawa, H.; Kurosawa, S.; Kobayashi, K.; Kashima, K.; Hirokawa, T.; Yoshimi, Y.; Yoshimoto, M.; Hirotsu, T.; Miyake, J.; Tanaka, H. *Materials Science & Engineering C-Biomimetic and Supramolecular Systems* **2000,** 12, (1-2), 49-54.

124. Wahlgren, M.; Arnebrant, T. *Trends in Biotechnology* **1991,** 9, (6), 201-208.

125. Sweryda-Krawiec, B.; Devaraj, H.; Jacob, G.; Hickman, J. J. *Langmuir* **2004,** 20, (6), 2054-2056.

126. Tanaka, M.; Mochizuki, A.; Motomura, T.; Shimura, K.; Onishi, M.; Okahata, Y. *Colloids and Surfaces a-Physicochemical and Engineering Aspects* **2001,** 193, (1-3), 145-152.

127. Baszkin, A.; Lyman, D. J. *J Biomed Mater Res* **1980,** 14, (4), 393-403.

128. Cheng, Y. Y.; Lin, S. H.; Chang, H. C.; Su, M. C. *Journal of Physical Chemistry A* **2003,** 107, (49), 10687-10694.

129. Tronin, A.; Dubrovsky, T.; Nicolini, C. *Langmuir* **1995,** 11, (2), 385-389.

130. Lord, M. S.; Stenzel, M. H.; Simmons, A.; Milthorpe, B. K. *Biomaterials* **2006,** 27, (4), 567-575.

131. Wertz, C. F.; Santore, M. M. *Langmuir* **2002,** 18, (3), 706-715.

132. Arai, T.; Norde, W. *Colloids and Surfaces* **1990,** 51, 1-15.

133. Vieira, E. P.; Rocha, S.; Pereira, M. C.; Mohwald, H.; Coelho, M. A. N. *Langmuir* **2009,** 25, (17), 9879-9886.

134. de Vos, W. M.; Biesheuvel, P. M.; de Keizer, A.; Kleijn, J. M.; Stuart, M. A. C. *Langmuir* **2008,** 24, (13), 6575-6584.